Dressel, I., Cacace, M., Scheck-Wenderoth, M. (2016): Coupled thermo-mechanical 3D subsidence analysis along the SW African passive continental margin. - *Arabian Journal of Geosciences*, *9*.

DOI: http://doi.org/10.1007/s12517-016-2407-9

Coupled thermo-mechanical 3D subsidence analysis along the SW African passive continental margin

Ingo Dressel*[1,2], Mauro Cacace[1], Magdalena Scheck-Wenderoth[1,2]

1 German Research Centre for Geosciences – GFZ, Helmholtz Centre Potsdam, Germany

2 RWTH Aachen, Germany

*Corresponding author: dressel@gfz-potsdam.de, German Research Centre for Geosciences – GFZ, Helmholtz Centre Potsdam, Germany, Section 4.4, Telegrafenberg, 14473 Potsdam, Germany. Tel.: +49 331 288 1792 Fax: +49 331 288 1349

Keywords: 3D modelling, passive continental margin, vertical movements, decoupling of the lithosphere

Abstract

Sedimentary basins along the SW African margin deliver information about processes, which occurred in the past and serve as a good starting point for reconstructing the margin's evolution. By integrating detailed information on the present-day configuration of the SW African margin into a 3D thermo-mechanical forward modelling framework, we attempt a margin-wide reconstruction of its subsidence history since its onset during breakup.

The 3D forward modelling approach as applied on the SW African margin area makes use of the coupling between thermal relaxation of the lithosphere and flexural isostatic balance in response to sediment deposition and build-up of thermal stresses during lithosphere cooling.

On the one hand, our results provide useful information about the behavior of the lithosphere during break-up and the subsequent post-rift phase. On the other hand, restored

paleobathymetries for specific time intervals during the post-rift evolution give evidence for possible uplift events superposed on the long-term subsidence history of the margin. Restored paleobathymetries are in agreement with conclusions derived from former studies and provided strong indications for the presence of a rather heterogeneous crustal configuration of the margin marked by a mechanical decoupling of the upper and lower crustal domains during most of the rifting phase.

1 Introduction

Several tectonic processes (i.e. ridge push from the spreading of the South Atlantic Ocean and deep mantle convective instabilities) have affected the thermal and mechanical configuration of the SW African continental margin since the breakup of Gondwana (approximately 125 Ma ago). As a result, the margin underwent a rather complex subsidence evolution characterized by a general deepening of the seafloor superimposed by local phases of upward vertical movements of the basement (e.g. Burke 1996; Guillocheau et al. 2013; Gurnis et al. 2000; Jackson et al. 2005; Nyblade and Robinson 1994). Understanding the dynamics of interaction among these processes and their effects on the thermo-mechanical configuration of the margin is therefore crucial to deepen our current knowledge of the geodynamic history of the sedimentary basins and its relation to the formation and maturation of their georesources. Previous studies mainly focused on characterizing the margin's configuration (e.g. Bauer et al. 2000; Gladczenko et al. 1998; Maystrenko et al. 2013; Paton et al. 2008), post-breakup vertical movements (Dressel et al. 2015; Japsen et al. 2012), sedimentation history and tectonic evolution for specific areas (e.g. Hirsch et al. 2007, 2009, 2010; Stewart et al. 2000; Broad et al. 2006; Uenzelmann-Neben et al. 2007; Brown et al. 1995). However, apart from some recent efforts (Braun et al. 2013; Rouby et al. 2013), these studies usually neglected to consider thermo-mechanical feedback effects on the subsidence and uplift processes along the continental margin. Additional work has been focused towards a quantification of the surface

expression of mantle dynamics (e.g. Burov and Guillou-Frottier 2005; Burov et al. 2007; Burov and Cloething 2007; Burov and Gerya 2014; Moucha and Forte 2011; Faccena and Becker 2010; Flament et al. 2013). Although these investigations provided useful insights into the dynamics of the deep mantle and its interactions with surface deformation processes, they usually relied on first order geodynamic principles thus hampering to link modelling results to available observations on the present-day margin configuration.

In the present study, we carry out a 3D thermo-mechanical subsidence analysis of the SW African margin (Figure 1) by taking into account the coupling between thermal cooling of the lithosphere, incremental and time varying loading by active sedimentation and their effects on the flexural behavior of the lithospheric plate. Similar to the work on 2D flexural modelling by Millán et al. (1995), we based our 3D forward modelling on detailed information available on the present-day configuration of the major basins along the SW African margin as summarized in a comprehensive 3D geological model by Maystrenko et al. (2013). In the final stage of the study, the results of the forward modelling are "validated" against available observations on the present-day bathymetry. At this stage, the aim is not to minimize the misfit between observations and model results by "ad hoc" tuning of the model parameters. Differences between model results and observation rather serve to lead a final discussion centered on additional processes that likely affected the margin evolution and the influence of which is neither directly stored in the sedimentary archive nor included in the modelling approach. Therefore, the advantage of the work stems not only from describing a 3D margin-wide thermo-mechanical model of its subsidence evolution, but by integrating detailed information of the sedimentary configuration as constrained at present, it also provides a data-driven approach to assist any reconstruction of the geodynamics of the margin since its formation.

2 Model parametrization and input data

Information about the sedimentary sequences as well as the deeper crustal and lithospheric mantle configurations have been summarized in a 3D structural model by Maystrenko et al. (2013). The model is based on different types of available data comprising seismics and seismological data, wells and it was finally constrained by 3D gravity modelling. We make use of grid-files as derived from this model to carry out our 3D forward modelling study. The rather complex sedimentary and crustal architecture of the SW African margin is exemplarily illustrated in Figure 2 along cross-sections running along each of the three main sedimentary basins.

The model differentiates between four major sedimentary units, each confined by horizons representing major unconformities: (1) syn-rift (base Aptian – top basement), (2) post-rift I (base Aptian – base Turonian), (3) post-rift II (base Turonian – base Cenozoic) and (4) post-rift III (base Cenozoic – seafloor). Clastic sediments comprising mainly sandstone and claystone as well as few shales and subordinate limestone dominate the entire sedimentary succession. In contrast to the African margin north of the Walvis Ridge, there is no evidence for salt deposition and halokinetics in the study area (Gladczenko et al. 1998; Karner and Driscoll 1999; von Nicolai et al. 2013).

Figure 3 illustrates isopach maps for all individual units resolved in the present study, showing their spatially varying thickness distribution throughout the area. Additionally, in Figure 4 we illustrate exemplarily synthetic wells chosen for three representative locations that will be used to discuss details of the subsidence evolution in the following chapters. This information is here added in order to better understand the distribution of the sediment in each of the major sedimentary basins. According to both Figures (3 and 4) it becomes obvious that the northern part of the SW African margin (Walvis Basin) and the southern part (Orange Basin) accommodate the thickest syn-rift unit and post-rift units. By contrast, the area in between (Lüderitz Basin) stores the thinnest sedimentary units but the deepest basement.

Furthermore, as shown also in Figure 2 the model by Maystrenko et al. (2013) differentiates the crust between domains of high-density and high-shear wave velocity embedded in a rather homogeneous crystalline crust. Thybo and Artemieva (2013) propose underplating along volcanic rifted continental margins during late stages of rifting and breakup but not post-breakup. For the reason that our study focusses on the margin evolution during the post-rift phase considering coupled thermo-mechanical processes, we assume these lower crustal bodies to have been emplaced pre-breakup. This assumption enables us to consider the crustal domain as a homogeneous layer (down to the crust-to-mantle boundary (Moho) of Maystrenko et al. 2013) for which an average density has been imposed (Table 1); however, an attempt to quantify the differences in the paleobathymetric evolution has been carried out and is further discussed in the discussion-part. The other geological layers included in the study comprise a lithospheric mantle overlying an iso-viscous asthenospheric layer. The latter has been implemented in the modelling for mainly numerical reasons in order to buffer the basal thermal input within the model domain. This was deemed necessary because of the choice of a thermal basal boundary, adopted, which consists of a fixed temperature rather than of a heat influx in the model domain. Therefore, the presence of such an adiabatic layer across the base of the model will guarantee a constant heat input from the bottom into the model thus avoiding possible boundary effects affecting the transient cooling of the system. Table 1 summarizes the relevant properties adopted for all layers in the forward modelling. As the focus of the present study is to reconstruct the subsidence evolution of the continental margin of SW Africa, the continent-ocean boundary (COB) after Pawloski (2008) is used to define the extent and boundary of the continental margin.

3 Methods

We follow a 3D thermo-mechanical approach (Cacace and Scheck-Wenderoth 2014) to model the post-rift evolution of the SW African margin taking into account details of the dynamic

coupling between sedimentation, lithospheric flexure and thermal contraction on the resulting subsidence. Figure 5 schematically illustrates the basic workflow. In the present study, we do not attempt any modelling of the rifting stage predating breakup. Instead, we introduce such a rifting event in terms of an initial destabilization of the thermo-mechanical configuration under pure shear and uniform stretching (McKenzie 1978). The starting model at equilibrium consists of a uniform crust (35 km thick) overlying a lithosphere (125 km thick). These values have been chosen because they represent present-day thicknesses as constrained for the lithosphere near the continental margin, therefore not affected by any stretching kinematics. Figure 6 illustrates a map showing the variations in the stretching factor considered in the modelling to destabilize the input model geometry. Stretching factor is here defined as the ratio between the crustal thickness at equilibrium (35 km) and the thickness observed at present-day, the latter being derived based on the 3D structural model as described in the previous paragraph. Following McKenzie (1978), instantaneous stretching of the lithosphere results in crustal and mantle thinning thus inducing a first stage of (syn-rift) subsidence and a thermal destabilization of the lithosphere.

The obtained geometric and thermal configuration is then used as initial conditions for forward modelling the post-rift evolution of the margin. Following our approach, subsidence results from flexural deformation of the lithospheric plate as induced by mechanical stresses during active sedimentation as well as by thermal stresses during cooling. Worth mentioning is, that these two processes are not solved independently, but are considered as dynamically coupled by means of a staggered iterative approach for solving the system of algebraic equations describing 3D conduction and advection and 3D beam flexure. Dynamic coupling is imposed in terms of a time and spatially varying flexural rigidity of the lithosphere taking into account both thermal and mechanical contributions. According to variations in the flexural rigidity of the plate, the deformation and subsidence of the continental margin varies in space and time and has a feedback effect on the thermal and mechanical evolution of the model.

For each time step, first the thermal field is solved by means of a bilinear Finite Element approximation of the following equation:

$$(\rho c_p)\frac{DT}{Dt} = \boldsymbol{\nabla}\cdot(k\nabla T) + H \quad (1)$$

where ρ is the rock density, c_p is the isobaric heat capacity, T is temperature, k is the thermal conductivity, and H is the amount of heat produced within the rock by decay of radiogenic elements. $\frac{DT}{Dt} = \frac{\partial}{\partial t} + (\mathbf{v}\cdot\nabla)$ is the total (Lagrangian) derivative, with $\mathbf{v}$ representing the sedimentation rate, here included to take into account advective heat transport component by sedimentation. Two sets of boundary conditions are imposed in order to close the system of equations. Temperature along the topmost surface, representing the seafloor, is kept fixed at T=5°. Worth to mention is that the geometry of this upper boundary does not remain constant during the simulation but it varies in time according to the sedimentation and subsidence history. The base of the mantle lithosphere is described by a partial melt isotherm for which a value of 1,350°C has been chosen. The topology of this isotherm is not maintained fixed, but it varies during the entire simulation depending on the cooling path followed by the lithospheric plate. Within the lowermost asthenosphere an adiabatic thermal gradient of 0.3°C km^{-1} is maintained with a reference potential temperature of 1,350°C. The imposed initial thermal configuration is calculated based on the model geometry at the beginning of the post-rift stage, thereby taking into account thermal destabilization as induced by uniform lithospheric stretching. Time discretization is performed via a Crank-Nicholson implicit scheme within a constant time stepping of 1 Myr.

Variations in the thermal field leads to the development of thermal stresses, which are then parameterized in terms of a bending moment and in-plane torque. The latter are added to the couple of moment-torque determined by sedimentation in order to solve for the 3D flexural equation (e.g. Kooi et al. 1989; Van Wees and Cloething 1996):

$$\nabla^2 M + \nabla(\mathbf{N}\cdot\nabla\omega) - K\omega = q - \nabla(\mathbf{N}\cdot\nabla\omega_0) \quad (2)$$

where M is the total plate bending moment (taking into account both mechanical and thermal processes), **N** is the net horizontal force component acting on the plate, ω is the deflection, K is the module of a linear elastic Winkler foundation imparting a normal traction to the base of the plate and ω_0 is an initial vertical displacement for a stress-free preloaded stage.

Though possible to parameterize the flexural rigidity via a rheological approach (i.e. based on strain rate independent yield strength envelope concept), in the present study, we opted for a relatively simpler approximation and we parameterized the flexural rigidity by means of a specified isotherm (e.g Burov and Diament 1995; McKenzie and Fairhead 1997; Watts 1992). For the latter a value of 450°C has been chosen, as this temperature roughly corresponds to the transition between brittle and ductile behavior at pressure and temperature conditions typically encountered at crustal level. Worth noticing, that this approach fails to account for stress (re)distribution within the plate during subsidence, and therefore flexural rigidity values calculated should be considered as upper bounds.

Apart from the syn-rift sediments which are deposited instantaneously soon after lithospheric stretching, post-rift sedimentation is introduced in the modelling as a gradual process (in 1 Myr steps). Sediments are deposited during a time window of finite duration. At this purpose, we follow the age subdivision after the chronostratigraphy by Broad et al. (2006) with a modification of the most recent timescale after Cohen et al. (2013). Table 1 illustrates the temporal subdivision adopted to include sedimentation in the forward modelling. In the present model we do not consider any external tectonic forcing, while we do integrate the contribution to the bending as induced by sea-level variations following the global dataset provided by Haq et al. (1987).

4 Results

4.1 Thermal evolution

Since the breakup of Gondwana the thermal field across the SW African continental margin changed strongly. Initial thermal destabilization during rifting went along with high heat flow related to stretching and breakup manifested in a shallow thermal LAB and elevated isotherms across the margins. At the end of the syn-rift phase (Figure 7) the 1,350°C isotherm, is as shallow as -35 km at the COB whereas its depth rapidly increases while moving towards the continental domain reaching values up to about -125 km at the coastline. Local positive thermal anomalies occur beneath both the Walvis and Orange Basins, areas that are characterized by relatively thick syn-rift sediments (Walvis Basin ~3 km; Orange Basin ~5 km; Figure 3). Here, heat retained within the sedimentary blanket causes higher temperatures resulting in LAB reaching values up to -50 km depths. By contrast, beneath the Lüderitz Basin the presence of a relatively thin sedimentary cover (~1 km; Figure 3) affect less significantly the overall thermal gradients as imposed by the thermal boundary conditions. As a result, the temperature field gradually and continuously decreases towards the interior domains of the African continent.

Cooling of the initial thermal anomalies at the onset of rifting continues throughout the entire post-rift evolution of the margin with a thermal configuration reaching approximately steady-state conditions at present-day (Figure 8). The retarding effects by sediment thermal blanketing are also visible in the present-day thermal configuration of the margin, which is characterized by relatively higher temperatures located beneath the three major depocentres of sedimentation. Since the amount of heat retained within the sedimentary cover scales linearly with the amount of sediment deposited, areas that underwent extensive sedimentation during the post-rift evolution are characterized by the highest temperatures. Indeed, this effect is most pronounced beneath the Orange Basin, where the greatest amount of post-rift sediments (around 6 km; Figure 3) has been deposited.

4.2 Evolution of the effective elastic thickness (EET)

By influencing rates of lithospheric cooling, the presence of a sediment cover of varying thickness exerts also a direct control on the mechanical behavior of the lithosphere. Consequently, thermal blanketing, causing higher than normal temperature conditions at the base of the infill, also affects the flexural rigidity of the lithosphere (here parametrized in terms of the 450°C isotherm). These aspects are schematically summarized in Figure 9, which shows the evolution of the flexural rigidity of the lithosphere in terms of Effective Elastic Thickness (EET) variations during the different post-rift stages. The EET within the study areas varies significantly during the 125 Ma after breakup. This is particularly the case within the first ~40 Myr of the post-rift evolution, during which time EET variations along the continental margin are the largest.

Given the linear relationship between the lithospheric thermal field and the corresponding flexural state, variations in modelled EET structurally correlate with temporal changes in the thermal configuration across the margin. The initial stages in the post-rift evolution are characterized by the presence of a higher, in magnitude, thermal anomaly as inherited from the rifting and therefore show a highly variable thermal configuration. Conductive cooling within the plate, smooths thermal destabilization with time thus reducing gradients in the flexural rigidity accordingly. At the beginning of post-rift phase I the calculated EET amounts to 12 km at the COB and 20 km along the coastline (Figure 9a). The Walvis and Orange Basin are characterized by an EET of about 12 km while the Lüderitz Basin has a thicker EET of about 18 km. 25 My after the breakup the EET has a thickness of 20 km at the African coastline and 20 km in the area of the COB (Figure 9b). Calculated EET values show only moderate variations during the remaining phase. This final period is characterized by a thickening trend in the area of the COB (maximum values up to 25 km at 85 Ma, 30 km at 67 Ma, 35 km at 25 Ma, 37 km at the present-day), whereas the EET remains almost constant (20 km) in the coastal areas (Figures 9c-9f). The sedimentary basins are also characterized by a general thickening of the EET. Accordingly, the Walvis Basin has an EET of 21 km at 85 Ma,

23 km at 67 Ma, 25 km at 25 Ma and 27 km at the present-day. More to the south, the Lüderitz Basin is marked by 20 km of EET at 85 Ma, 21 km at 67 Ma, 23 km at 25 km and 26 Ma at the present-day. The Orange Basin which has initially the thinnest EET reaches an EET of 18 km at 85 Ma, 20 km at 67 Ma, 26 km at 25 Ma and 29 km at present-day.

The effects of sedimentation on the resulting thermal field and consequently flexural rigidity variations are also captured by the evolution of calculated EET through time during the post-rift evolution of the margin. By inspecting the different maps shown in Figure 9, it can be noticed that during early stages (until ~67 Ma) the southern domain of the study area is characterized by smaller EET thickness values than the domains further to the north. This is in agreement with higher volumes of sediments being deposited during this time window especially in the area of the Orange Basin. The gradual northward shift in the main depocentres of sedimentation (Maystrenko et al. 2013) spatially correlates with a change in the EET configuration during the last phases of the post-rift evolution of the margin and a general deepening within the southern domain.

4.3 Subsidence of the passive continental margin

The modelled overall subsidence of the passive continental margin is schematically illustrated in Figure 10. This figure exemplarily shows the amount of load induced, thermal as well as the sum of the total subsidence since the breakup of the South Atlantic Ocean (125 Ma) for three synthetic wells located beneath the major basins. The thermal subsidence curves show an exponential trend with rapid cooling during the first ~40 Myr after breakup. During the remaining ~85 Myr cooling rates slow down thus resulting in a flattening of the thermal subsidence curves. While the Walvis Basin and the Orange Basin experienced a similar amount of of thermal subsidence (~2,200 m) the Lüderitz Basin has a smaller amount of thermal subsidence of about 900 m.

A shift in sediment deposition is clearly visible in all subsidence curves. At 67 Ma the area of the Orange Basin is characterized by a strong decrease in load induced subsidence (the area between the thermal subsidence curve and the total subsidence curve) which is in contrast to the high amount of load induced subsidence during the first 58 Myr after breakup. Nevertheless, the Orange Basin experienced the highest amount of load induced subsidence (~3,200 m) compared to the amounts of load induced subsidence of the Walvis Basin and Lüderitz Basin. The latter two basins are characterized by a minor amount of load induced subsidence (Walvis Basin ~1,800 m and Lüderitz Basin ~700 m). This trend scales linearly with the amount of sedimentation observed in the three basin areas.

The total subsidence calculated sums up to approximately ~5,400 m in the Orange Basin, ~-4,000 m in the Walvis Basin m and ~1,600 m in the Lüderitz Basin.

Comparing those subsidence curves with the subsidence curves along the SW African margin using local isostatic compensation according to Dressel et al. (2015) shows differences in the thermal subsidence curves as well as in the total subsidence curves. These differences stems from differences in the two approaches. Indeed, the study by Dressel et al. (2015) do not consider either thermo-mechanical coupling or a spatio-temporal varying strength of the lithosphere. Regarding the thermal subsidence curves, such coupling results in a larger amount of thermal subsidence due to dynamic interaction between thermal cooling and sediment deposition. By contrast, the total amount of subsidence is smaller for the 3D case than if based on calculation assuming local isostatic compensation (i.e. constant EET=0). This aspect is related to the fact that local isostatic compensation, neglecting a finite rigidity of the lithospheric plate, corresponds to the end-member case of a weak lithosphere. Whereas, the consideration of a finite in magnitude and laterally varying EET, by taking the effective strength of the lithosphere into account, results in a stronger configuration of the plate, thus resulting in less deflection.

4.4 Paleobathymetric evolution

Using the information derived from the modelled thermal and mechanical (EET) evolution and linking it to the sedimentation history as constrained by the input 3D geological model allows restoring paleobathymetries for different time spans during the entire evolution of the continental margin.

Figure 11 illustrates paleobathymetric maps as calculated from the 3D forward numerical simulation at different times during the evolution of the margin in accordance to the resolution of the model used: 125 Ma (soon after the rifting ceased), 93 Ma and 67 Ma. The bathymetry obtained after instantaneous deposition of syn-rift sediments (125 Ma) shows already positive topography up to 900 meter above sea level (m.a.s.l.) in the norther domain and 500 m.a.s.l. in the south as well as in the central parts. Modelled positive paleotopographies at 93 Ma amounts to 300 m.a.s.l. in the north, 50 m in the central part and 400 m.a.s.l. in the south and finally to 900 m.a.s.l. at 67 Ma, both, in the north as well as in the south but only 200 m.a.sl. in the central part, after the sediments of post-rift phase I and II have been deposited. The presence of these positive paleotopographies during the post-rift evolution calls for additional processes that likely affected the geodynamic history of the margin and that have been not considered in the present study. These are discussed in details in the paragraph that follows.

5 Discussion

5.1 Implications for uplift

In an attempt to "validate" the modelling efforts, we compare observed present-day bathymetry of the SW African margin to the one predicted by the model. The model predicts a general deepening of the bathymetry towards the COB, which is in agreement with the general trend observed at present-day; however, local differences between modelling results and observations are found beneath the three major basins. In more detail, modelled present-

day bathymetry beneath the continental margin amounts to about 1,000 meters below sea level (m.b.s.l.) in average and increases to about 2,500 m.b.s.l. to 3,000 m.b.s.l. at the COB. This is comparable to the present-day observed bathymetry at the COB with an amount of about 3,000 m.b.s.l, whereas areas of main sedimentation are characterized by positive paleotopographies up to 1,700 m.a.s.l. in the north, 450 m.a.s.l. in the south and about 850 m.a.s.l. in the central part (Figure 12). Within these domains, modelling results are therefore in conflict with the preserved configuration and thickness distribution of the sedimentary cover, which indicates ongoing subsidence throughout the post-rift evolution of the margin.

On the one hand, dissimilarities observed between model results and observations can be explained, at least partly, by the occurrence of phases of margin uplift throughout the post-rift evolution of the margin. Indications for uplift events have been discussed by Kuhlmann et al. (2011) and Paton et al. (2008) using mapped erosional unconformities in the sedimentary succession. Furthermore, regarding the temporal occurrence of uplift events in southern Africa, Séranne and Anka (2005) discuss the Sennoninan-phase of uplift starting in the Turonian. This event temporally correlates with the obtained positive paleobathymetries of post-rift phase II (93 Ma until 67 Ma; Figure 11). In addition, our results are in accordance to previously published results based on apatite fission tracked analysis by Kounov et al. (2013) which pointed to regional uplift during the time interval from 100-65 Ma. This temporal correlation between our modelling results and observations derived from seismic data and additional thermochronology strongly suggest the obtained positive paleotopographies to represent uplift events occurring during the post-rift evolution of the margin. According to our results, we would obtain ~450 m of uplift for the northern and southern area for the duration of post-rift phase II. Comparing this amount with the suggested denudation rate of 25 m/Myr as presented by Kounov et al. (2013) for the Late Cretaceous yields the same range of uplift. Additionally, magnitudes of this uplift event are in agreement with Kuhlmann et al. (2011),

who determined 930 m of erosion, though these results concern the specific area of the Orange Basin, and are therefore difficult to extrapolate margin wide.

The amount of deduced relative uplift for the final post-rift phase (post-rift phase II: 67 Ma until present) is 800 m in the Walvis Basin and 650 m in the Lüderitz Basin, whereas the area of the Orange Basin is now subsiding. Our results agree with previous conclusions by Stollhofen et al. (2014), suggesting Pliocene-Pleistocene uplift based on a sedimentological study of a fan delta in Namibia. A study by Burke et al. (1996) proposed that the southern African continent has been uplifted since 30 Ma, a conclusion, which finds a confirmation in our findings, at least for the northern part of our research area. Furthermore, Colli et al. (2014) also suggested major uplift events during the Oligocene-Miocene, which are again confirmed by our findings for post-rift phase III. The latter two studies proposed mantle processes as responsible for the observed uplift. Similarly, investigations on dynamic topography (e.g. Flament et al. 2013 or Lihtgow-Bertelloni and Silver 1998) indicated significant vertical motions by mantle flow. According to Braun et al. (2014), denudation onshore Africa was rather caused by a tilting of the African continent in response to a super plume.

Therefore, it is likely that the observed positive topographies along the margin might be explained by episodic tectonic uplift movements and sediment erosion. This aspect is consistent with several studies (e.g. Burke et al. 1996; Moucha and Forte 2011; Patridge and Maud 1978), which pointed to episodically uplift since Mesozoic times in areas near the coastal margins.

On the other hand, focusing only on the post-rift phase I (125 Ma – 93 Ma), by subtracting the resulting paleotopographies at the top of the syn-rift phase (125 Ma) and at the top post-rift phase I (93 Ma) yields an amount of relative subsidence during this stage. The amount of relative subsidence range between 600 m in the Walvis Basin, 450 m in the Lüderitz Basin and 100 m in the Orange Basin. Computed subsidence is nevertheless too small to compensate

for syn-rift sediments, which have been accumulated, thus resulting in a positive paleotopography at the end of post-rift phase I. Given the above discussion, the observed positive paleotopographies can be related to a structural inheritance (weakening of the lithosphere) derived from the rifting that our study could not resolve. If this had been the case, a weaker lithosphere during rifting would have respond to the coeval deposition of the thick sequence of syn-rift sediments by higher wavelength of deflection, thus providing a thermo-mechanical intrinsic solution to the missing accommodation space soon after the rifting event ceased. This would also be in agreement with a previously study by Hirsch et al. (2010), which supported continuous subsidence during the youngest post-rift time interval for the Orange Basin. However, to test and quantify this hypothesis would require a more detailed investigation of the rifting dynamics of the margin, a subject that goes beyond the scope of the present study.

5.2 Implications for additional subsidence components

As mentioned in the chapter previous chapter, the calculated positive paleotopographies at 125 Ma, soon after the rifting event, already point to elevations above sea level. As there are no observational evidences indicating uplift during the syn-rift phase and the duration of the syn-rift phase is unknown, it is likely that calculated positive paleotopographies result from limitations of the pure shear and uniform, instantaneous stretching model approximation adopted to model the rifting event. Our results clearly point to the fact that calculated syn-rift subsidence from uniform stretching of the lithosphere could not create enough accommodation space to store the total amount of syn-rift sediments.

To provide a quantitative basis to our discussion, we carried out a sensitivity analysis in which we investigate first-order differences in the syn-rift configuration and their effects on the margin geometry. In a first attempt, we consider variation in the initial configuration of the crust and lithospheric mantle, by considering 40 km thickness for the former (instead of

the 35 km assumed earlier) and 130 km for the latter (instead of 125 km). According to the new configuration, the remaining missing subsidence still attains of up to ~500 m (Figure 13). For the reason that this configuration does also not yield enough accommodation space and the fact that 35 km crustal and 125 km lithospheric thickness represent areas at the African margin which are not affected by stretching we consider these values more appropriate. In addition, the reconstructed depth along the COB using this configuration coincides with the present-day depth at the COB. Consequently, our obtained missing subsidence rather points to intrinsic limitations in the physics behind uniform lithospheric stretching, such as decoupling of the lithosphere, rather than on the initial lithospheric configuration as a source of error. Similar conclusions were derived from a previous study by Hirsch et al. (2010) centered on the Orange Basin. According to their subsidence analysis, the observed tectonic history and maturation of organic matter could not be reproduced by assuming uniform stretching of the lithosphere. Comparing these aspects to other conjugate margins leads to further insights on the rifting processes. Accordingly, the study by Espurt et al. (2012) analyzing the Australian and Antarctic conjugate margins, showed how complex the rifting procedure may occur. These authors propose a rather symmetric geometry, due to pure shear, of the rift system at the crustal- as well as lithospheric scale during the initial stretching, followed by simple shear deformation shortly before breakup. The latter is justified by Espurt et al. (2012) showing that the ductile lower crust acting as a zone separating the brittle upper crust and the lithospheric mantle. Given this discussion, the SW African passive margin could also underwent such a rifting history in which the later decoupling causes the ductile flow of the crust with additional subsidence as a result.

As discussed by Burov and Diament (1995) and Burov and Poliakov (2001) the mechanical properties of the oceanic lithosphere can be approximated by a single layer while the continental lithosphere may be composed of mechanically decoupled layers. Mechanical decoupling at crustal and mantle levels may cause horizontal ductile flow in the lower crust

that would, in turn, affect the subsidence history. The net result of these dynamics is additional subsidence mainly beneath areas of lower crustal flow. This could partly explain the observed positive paleotopographies, thus indicating that lower crustal flow might have played a prominent role during at least the first stage of the post-rift evolution of the SW African margin.

Similar conclusions were derived from a study by Huismans and Beaumont (2011). In their study, they were able to reproduce a margin setting as typically observed in the south Atlantic by means of a model in which the upper and lower lithosphere are decoupled during extension due to asthenospheric inflow. Based on their result, they concluded that depth-dependent rather than uniform lithospheric stretching would occur in these settings. A rheologically stratified lithosphere would increase the amount of subsidence, especially during early stages after the rifting and could therefore provide the "missing accomodation space" for the syn-rift sediments. Additionally, the model by Huismans and Beaumont (2011) was also used to explain the dynamics of underplating due to mantle flow within a mechanically decoupled lithosphere. This last aspect brings some interesting similarities to the crustal configuration as constrained for the SW African margin, which is characterized by areas of high-density and high-shear wave velocity at different locations (Maystrenko et al. 2013). According to the architecture of the margin, as shown in Figure 2, high-density bodies and high-shear wave velocity bodies underlay the continental crust. To derive the modelling with focus on the post-rift phase we assume these bodies as part of the crystalline crust which is in agreement with Thybo and Artemieva (2013) who proposed that many passive margins experienced underplating during the late stages of rifting and breakup. However, the heterogenous crustal configuration according to Maystrenko et al. (2013) and the discussion of underplating by Huismans and Beaumont (2011) point to underplating as coeval to the rifting rather than postpone to the post-rift phase.

Based on the discussion above, in a second step of our sensitivity analysis, we investigate the effects of underplating occurring after the main phase of rifting on the margin evolution. Therefore, to calculate the initial subsidence without these lower crustal bodies we impose the lower crustal bodies as part of the mantle but not of the crystalline crust. Figure 14 shows the top of the syn-rift unit after calculating the syn-rift subsidence and depositing the syn-rift sediments. Similar to the scenario with lower crustal bodies as part of the continental crust we still obtain positive paleotopographies, though they are smaller in magnitude (~700 m). Accordingly, and based on the results derived from our study we can conclude that it is likely that the positive paleotopographies result from processes during the syn-rift (possible decoupling of the lithosphere).

5.3 Limitations

This work challenges conclusions derived from previous studies that proposed a relative uniform EET distribution close to an average value of 25 km (Stewart et al. 2000). Our results call for a highly variable flexural state of the lithosphere being characterized by values of EET, which are generally lower than the 25 km average of Stewart et al. (2000) during most of the post-rift stage. Despite current assumptions in parameterizing the flexural state of the lithosphere by an isotherm, our results of ~20 km at the unstretched SW African coast are in close agreement with estimates based on gravity anomalies providing evidence for EET values lower than 25 km (McKenzie and Fairhead 1997). Nevertheless, differences between modelling results and observations for the post-rift phases can be discussed in terms of some basic physical assumptions in our modelling approach that affect our results. As stated above, for the present study, we parameterize the EET by means of a specific isotherm (T=450°), the latter representing a common value adopted in several flexural studies, e.g. Rouby et al. (2013) and Watts (1978). However, while this value could be considered as a proxy for the flexural rigidity of oceanic lithosphere, it might lead to an overestimation of the effective

flexural state for the continental counterpart. As an example, Burov and Diament (1995) suggested an isotherm closer to 600°C to best represent the EET both for old oceanic and continental lithosphere. In an attempt to perform a sensitivity analysis, we show in Figure 15 the differences of the reconstructed bathymetry, by assuming 600°C and 450°C, respectively, as the lower boundary for the EET. Inspecting Figure 15 it becomes clear that the former yields to higher amounts of positive paleotopography along the continental margin (up to 400 m). Observed differences should be related to a decrease in the amount of load induced subsidence for a 600°C isotherm, which leads to a stiffer lithosphere than for the 450°C isotherm case characterized by a reduced amplitude of flexure and by an increase in the wavelength of deformation. On the base of these results, we could conclude that the missing subsidence in the modelling cannot be solely explained by this assumption. Furthermore, approximating the EET by means of a constant, though varying in time isotherm, implicitly assumes an overall thermal control on the mechanical properties of the lithosphere, which represents a rather crude approximation for continental lithosphere (Burov and Diament, 1995). A continental lithosphere, which is cooling after a thermal event, will result in a plate elastic thickness that will increase in magnitude as the thermal anomaly is relaxed, in a similar way as for the oceanic case. Although this behavior can be modulated by mechanical softening related to viscous relaxation, it fails to account for possible stress redistribution within the plate, which might lead to overestimate the EET of the plate. This in turn might lead to an overly stiffer lithosphere, therefore less prone to subside under active sedimentation. A more detailed investigation based on a fully rheological parameterization of the EET is subject of ongoing work.

An additional assumption, which could have affected the conclusions derived from our analysis, can be related to the value of potential mantle temperature adopted in the modelling for which a consensus among the geodynamic community is still lacking. While McKenzie et al. (2005) proposed a value close to 1,315°C, more recently Grose (2012) suggest a potential

mantle temperature of 1,400°C which was increased by Stein and Stein (1992) up to 1,450°C. In addition, Burov and Watts (2006) used 1,330°C while Parson and Sclater (1977) a slightly higher value of 1,350°C. In our study, we imposed a fixed value of 1,350°C, which represent an average of potential temperatures mentioned above. However, to further quantify the effects of varying this parameter, a sensitivity study has also been performed in which its value was gradually decreased down to 1300°C. The results of this analysis showed that changing the mantle potential temperature from 1350°C to 1300°C would cause a maximum difference of the positive paleotopographies of less than 20 m. Therefore, we can conclude that this, not well constrained parameter would likely play only a secondary role in affecting the geodynamic evolution of the SW African margin.

5.4 Potentials for geo-resources

The final part of the discussion focuses on implications derived from the modelling results on the potential for geo-resources formation and evolution. Through time, organic matter, deposited in the sedimentary basin, matures according to increasing temperature and pressure and may migrate into potential reservoirs for hydrocarbons. As the oil window is reached at a temperature of ~130°C (Bjørlykke 2010) this isotherm is an appropriate proxy for oil generation. Therefore, these temperatures are of primary interest within the major sedimentary basins. Our thermo-mechanical 3D forward modeling allows reconstructing the evolution of the oil window for oil-bearing sequences through time.

After Hartwig et al. (2012), the late Aptian and Albian black shales and organic rich dolomitic mudstones show a good source rock potential offshore southwestern Africa. The resolution of the input model does not resolve this unit in details, but it can be approximated by post-rift phase I unit which contains the oil-bearing sequence. Our post-rift phase I encompasses the sediments deposited from 125 Ma to 93 Ma. Consequently, the top of post-rift phase I is the base Turonian, which is about 7 Ma younger than the late Aptian and Albian blackshales.

The forward modelling allows predicting the migration of the 130°C isotherm in depth and through time with respect to the oil-bearing unit. According to our model resolution, we infer the depth to the 130°C isotherm for three time steps during the post-rift phase.

Post-rift unit I reaches 130°C in the central western part of the Orange Basin in a depth of about 2,950 m.b.s.l at 93 Ma. At 67 Ma, after the second post-rift phase has been deposited, the location of the oil window remains under the same area though it increases spatially and reaches shallower depth levels. Correspondingly, the depth to the oil window is about 2,900 m.b.s.l beneath a larger area of the central part of the Orange Basin. Finally, post-rift phase I unit is buried to the 130°C isotherm to a depth of about 4,000 m.b.s.l in the Orange Basin at the modeled present-day. The Lüderitz Basin is now characterized by about 3,400 m.b.s.l. to the depth of the 130°C isotherm. Shallowest depths of about 2,000 m.b.s.l. to the oil window are obtained in the northern part of the Walvis Basin.

In comparison to the steady-state thermal model by Maystrenko et al. (2013), our modelled 130°C isotherm for today is located at shallower depths in the north, and at similar depths beneath the central part and greater depths in the south.

6 Conclusions

We have presented a margin-wide analysis of the post-rift evolution of the SW African margin by means of 3D thermo-mechanical forward numerical modelling techniques. Our approach permits to consider both, thermal cooling of the lithosphere and mechanical effects of sedimentation and their dynamic coupling on the resulting subsidence pattern. Furthermore, our modelling approach integrates available information about the configuration and geometry of the sedimentary units as well as information about the deeper crustal and lithospheric mantle domains as constrained at present. With respect to the thermo-mechanical coupling, we presented temporal and spatial variations in the EET (i.a. flexural rigidity) of the

lithosphere throughout the post-rift evolution of the margin. This aspect is explained as a response of the plate to temporal cooling and active sedimentation dynamics.

In addition to the new insights on the EET, we restore paleobathymetries. These paleobathymetries point to elevations above sea level. Discussing these positive paleotopographies with respect to the method used lead to suggest lower crustal flow during the syn-rift phase. Accordingly, future work should focus on the processes during the syn-rift phase rather than processes of the post-rift phase.

Acknowledgements

This project was funded by the German Research Foundation (DFG, grant no. SCHE 674/5-3) within the priority program South Atlantic Margin Processes and Links with onshore Evolution (SAMPLE; SPP 1375). We thank Yuriy P. Maystrenko for providing the thickness maps used in this study. Furthermore, we thank F. Roure and an anonymous reviewer for their constructive comments which helped to improve the manuscript.

References

Bauer K, Neben S, Schreckenberger B, Emmermann R, Hinz K, Fechner N, Gohl K, Schulze A, Trumbull RB, Weber K (2000) Deep structure of the Namibia continental margin as derived from integrated geophysical studies. J. Geophys. Res. 105:25,829–25,853

Bjørlykke K (2010) Petroleum Geoscience. From sedimentary Environments to Rock Physics. Springer, Heidelberg

Braun J, Deschamps F, Rouby D, Dauteuil O (2013) Flexure of the lithosphere and the geodynamical evolution of non-cylindrical rifted passive margins: Results from a numerical model incorporating variable elastic thickness, surface processes and 3D thermal subsidence. Tectonophysics 604:72-82. doi:10.1016/j.tecto.2012.09.033

Braun J, Guillocheau F, Robin C, Baby G, Jelsma H (2014) Rapid erosion of the Southern African Plateau as it climbs over a mantle supersell. J. Geophys. Res. Solid Earth 119:6093-6112. doi:10.1002/2014JB010998

Broad D, Jungslager E, McLachlan I, Roux J (2006) Offshore mesozoic basins. In: Johnson MR, Anhausser CR, Thomas RJ (eds.) Geology of South Africa. Geological Socienty of South Africa/Council for GeoScience, Pretoria, pp 553–571

Brown LF, Benson Jr JM, Brink GJ, Doherty S, Jollands A, Jungslager EHA, Keenan JHG, Muntingh A, van Wyk NJS (1995) Sequence stratigraphy in offshore South African divergent basins. An atlas on exploration for Cretaceous lowstand traps by Soeker (Pty) Ltd. AAPG, Studies in Geology 41

Burov E, Diament M (1995) The effective elastic thickness (Te) of continental lithosphere: What does it really mean? J. Geophys. Res. 100(B3):3905-3927

Burov E, Poliakov A (2001) Erosion and rheology controls on synrift and postrift evolution: Verifying old and new ideas using a fully coupled numerical model. J. Geophys. Res. 106(B8):26,461-16,481

Burov E, Guillou-Frottier L (2005) The plume-continental lithosphere interaction using a tectonically realistic formulation for the lithosphere. Geophys. J. Int. 161:469-490 doi:10.1111/j.1365-246X.2005.02588.x

Burov E, Watts AB (2006) The long-term strength of continental lithsophere: "jelly sandwich" or "crème brûlée". GSA Today, 16,1:4-10. doi:10.1130/1052-5173(2006)016<4:TLTSOC>2.0CO;2

Burov E, Guillou-Frottier L, d'Acremont E, Le Pourhiet L, Cloething S (2007) Plume head-lithosphere interactions near intrac-continental plate boundaries. Tectonophysics 343: 15-38. doi: 10.1016/j.tecto.2007.01.002

Burov E, Cloething S (2010) Plume-like upper mantle instabilities drive subdaction initiation. Geophys. Res. Letters 37:L03309. doi:10.1029/2009GL041535

Burov E, Gerya T (2014) Asymmetric three-dimensional topography over mantle plumes. Nature 513:85-89. doi:10.1038/nature13703

Burke K (1996) The African plate. South African J. Geol. 99:41–409

Cacace M, Scheck-Wenderoth M (2014) Different subsidence components at passive margins. Geophys. Res. Abstracts 16. EGU2014-5281

Coehen KM, Finney SM, Gibbard PL, Fan JX (2013) The ICS International Chronostratigraphic Chard. Episodes 36(3):199-204

Colli L, Stotz I, Bunge HP, Smethurst M, Clark S, Iaffaldano G, Tassara A, Guillocheau F, Bianchi MC (2014). Rapid South Atlantic spreading changes and coeval vertical motion in surrounding continents: Evidence for temporal changes of pressure-driven upper mantle flow. Tectonics 32:1304–1321. doi:10.1002/2014TC003612

Dressel I, Scheck-Wenderoth M, Cacace M, Lewerenz B, Götze HJ, Reichert C (2015) Reconstruction of the southwestern African continental margin by backward modeling. Mar. Pet. Geol. 67:544-555. doi:10.1016/j.marpetgeo.2015.06.006

Espurt N, Callot J-P, Roure F, Totterdell JM, Struckmeyer HIM, Vially R (2012) Transition from symmetry to asymmetry during continental rifting. an example from the Bight Basin-Terre Adélie (Australien and Antarctiv conjugate margins). Terra Nova 24:167-180. doi:10.1111/j.1365-3121.2011.01055.x

Faccena C, Becker T (2010) Shaping mobile belts by small-scale convection. Nature 465. doi:10.1038/nature09064

Flament N, Gurnis M, Müller RD (2013) A review of observations and model of dynamic topography. Lithosphere. doi:10.1130/L245.1

Gladczenko TP, Skogseid J, Eldhom O (1998) Namibia volcanic margin. Mar. Geophys. Res. 20: 313–341.

Guillocheau F, Dauteil O, Baby G, Robin C (2013) Uplift of the South Afrian Plateau: mantle-scale deformation, long wavelength relief growth and offshore sediment budget. Geophys. Res. Abstr. 15. EGU2013-12743

Gurnis M, Mitrovica JX, Ritsema J, van Heijst H-J (2000) Constraining mantle density structure using geological evidence of surface uplit rates: The case of the African superplume. Geochem. Geophys, Gesyst. 1. doi:10.1029/1999GGC000035

Grose CJ (2012) Properties of oceanic lithosphere: Revised plate cooling model predictions. Earth Plat. Sci. Lett. 333-334:250-264, doi:10.1016/j.epsl.2012.03.037

Haq BU, Hardenbol J, Vail PR (1987) Chronology of fluctuating sea levels since the triassic. Science 235:1156–1167

Hartwig A, Anka Z, di Primio R (2012) Evidence of a widespread paleo-pockmarked field in the Orange Basin: An indication of an early Eocene massive fluid escape event offshore South Africa. Mar. Geol. 332-334:222–234. doi:10.1016/j.margeo.2012.07.012

Hirsch KK, Scheck-Wenderoth M, Paton DA, Bauer K. (2007) Crustal structure beneath the Orange Basin, South Africa. South African J. Geol. 110:249–260. doi:10.2113/gssajg.110.2-3.249

Hirsch KK, Bauer K, Scheck-Wenderoth M (2009) Deep structure of the western South African passive margin - Results of a combined approach of seismic, gravity and isostatic investigations. Tectonophysics 470:57–70. doi:10.1016/j.tecto.2008.04.028

Hirsch KK, Scheck-Wenderoth M, van Wees JD, Kuhlmann G, Paton D A (2010). Tectonic subsidence history and thermal evolution of the Orange Basin. Mar. Pet. Geol. 27:565–584. doi:10.1016/j.marpetgeo.2009.06.009

Holtar E, Forsberg AW (2000) Postrift development of the Walvis Basin, Namibia. Results from the exploration campagin in quadrant 1911. In: Mello MR, Katz BJ (eds) Petroleum systems of South Atlantic margins: AAPG Memoir 73:429-446

Huismans R, Beaumont C (2011) Depth-dependent extension, two-stage breakup and cratonic underplating at rifted margins. Nature 473:74-78. doi:10.1038/nature09988

Jackson MPA, Hudec MR, Hegarty KA (2005) The great West African Tertiary coastal uplift: Fact or fiction? A perspective from the Angoland divergent margin. Tectonics 24, TC6014. doi:1029/2005TC001836

IOC, IHO, BODC (2013). Centenary Edition of the GEBCO Digital Atlas, published on CD-ROM on behalf of the Intergovernmental Oceanographic Commission and the International Hydrographic Organization as part of the General Bathymetric Chart of the Ocean; British Oceanographic Data Centre, Liverpool

Japsen P, Chalmers JA, Green PF, Bonow JM (2012) Elevated, passive continental margins: Not rift shoulders, but expressions of episodic, post-rift burial and exhumation. Glob. Planet. Change 90-91:73–86. doi:10.1016/j.gloplacha.2011.05.004

Karner GD, Driscoll NW (1999) Tectonic and stratigraphic development of the West African and eastern Brazilien Margins: insights from quantitative basin modelling. In: Cameron NR, Bate RH, Clure VS (eds) The Oil and Gas Habitats of the South Atlatnic. Geol. Soc. London, Spec. Publ. 153, 11-40.

Kounov A, Viola G, Dunkl I, Frimmel HE (2013) Southern African perspectives on the long-term morpho-tectonic evolution of cratonic interiors. Tectonophysics 601:177–191. doi:10.1016/j.tecto.2013.05.009Kuhlmann G, Adams S, Anka Z, Campher C, di Primio R, Horsfield B (2011) 3D Petroleum Systems Modelling Within a Passive Margin Setting, Orange Basin, Blocks 3/4, Offshore South Africa - Implications for Gas Generation, Migration and Leakage. South African J. Geol. 114:387–414. doi:10.2113/gssajg.114.3-4.387

Kooi H, Cloething S, Remmelts G (1989) Intraplate streses and the stratigraphic evolution of the North Sea Central Graben. Geologie en Mijnbouw 68:49-72.

Lithgow-Bertelloni C, Silver P (1998) Dynamic topography, plate driving forces and the African superswell. Nature 395:345–348

Maystrenko YP, Scheck-Wenderoth M, Hartwig A, Anka Z, Watts AB, Hirsch KK, Fishwick S (2013) Structural features of the Southwest African continental margin according to results of lithosphere-scale 3D gravity and thermal modelling. Tectonophysics 604:104–121. doi:10.1016/j.tecto.2013.04.014

McKenzie D (1978) Some remarks on the development of sedimentary basins. Earth Planet. Sci. Lett. 40:25–32

McKenzie D, Fairhead D (1997) Estimates of the effective elastic thickness of continental lithosphere from Bouger and free air gravity anomalies. J. Geophys. Res. 102(B12):27,523-27,552

McKenzie D, Jackson J, Priestley K (2005) Thermal structure of oceanic and continental lithosphere. Earth Planet. Sci. Lett. 233:337-349. doi:10.1016/j.epsl.2005.05.005

Millán H, Den Bezemer T, Vergés J, Marzo M, Muñoz JA, Roca E, Cirés J, Zoetemeijer R, Cloething S, Puigdefabregas C (1995) Paleo-elevation and effective elastic thickness evolution at mountain ranges: inferences from flexural modelling in the Eastern Pyrenees and Ebro Basin. Mar. Pet. Geol. 12 (8):917-928Moucha R, Forte AM (2011). Changes in

African topography driven by mantle convection. Nat. Geosci. 4:707–712. doi:10.1038/ngeo1235

Nyblade A, Robinson S (1994) The African superswell. Geophys. Res. Lett. 21,765-768

Parson B, Sclater JG (1977) An analysis of the variation of ocean floor bathymetry and heat flow with age. J. Geophys. Res. 82,5:803-827

Paton DA, di Primio R, Kuhlmann G, van der Spuy D, Horsfield B (2007) Insights into the Petroleum System Evolution of the southern Orange Basin, South Africa. South African J. Geol. 110:261-274. doi: 10.2113/gssajk.110.2-3.261

Paton DA, van der Spuy D, di Primio R, Horsfield B (2008) Tectonically induced adjustment of passive-margin accommodation space; influence on the hydrocarbon potential of the Orange Basin, South Africa. Am. Assoc. Pet. Geol. Bull. 92:589–609. doi:10.1306/12280707023

Patridge TC, Maud RR (1987) Geomorphic evolution of southern Africa since the Mesozoic. South African J. Geol. 90(2):179-208

Pawlowski R (2008) The use of gravity anomaly data for offshore continental margin demarcation. The Leading Edge 27:722–727. doi:10.1190/1.2944156

Rouby D, Braun J, Robin C, Dauteuil O, Deschamps F (2013) Long-term stratigraphic evolution of Atlantic-type passive margins: A numerial approach of interactions between surface processes, flexural isostasy and 3D thermal subsidence. Tectonophysics 604:83-103. doi:10.1016/j.tecto.2013.02.003

Scheck-Wenderoth M, Cacace M, Dressel I (2015) Multiple uplift phases inferred from the southwest African Atlantic margin. Geophys. Res. Abstracts 17. EGU2015-7230

Sclater J, Christie P (1980) Continental stretching: An explanation of the post-Mid-Cretaceous subsidence of the central North Sea Basin. J. Geophys. Res. 85:3711–3739

Séranne M, Anka Z (2005) South Atlantic continental margins of Africa: a comparison of the tectonic vs climate interplay on the evolution of equatorial west Africa and SW Africa margins. J. African Earth Sci. 43:283–300. doi:10.1016/j.jafrearsci.2005.07.010

Stein CA, Stein S (1992) A model for the global variation in oceanic depth and heat flow with lithospheric age. Nautre 359:123-129

Stewart J, Watts AB, Bagguley JG (2000) Three-dimensional subsidence analysis and gravity modelling of the continental margin onshore Namibia. Geophys. J. Int. 141:724–746

Stollhofen H, Stanistreet IG, von Hagke C, Nguno A (2014) Pliocene–Pleistocene climate change, sea level and uplift history recorded by the Horingbaai fan-delta, NW Namibia. Sediment. Geol. 309:15–32. doi:10.1016/j.sedgeo.2014.05.008

Thybo H, Artemieva IM (2013) Moho and magmatic underplating in continental lithosphere. Tectonophysics 609:605-619. doi:10.1016/j.tecto.2013.05.032

Uenzelmann-Neben G, Schlüter P, Weigelt E (2007) Cenozoic oceanic circulation within the South African gateway: indications from seismic stratigraphy. South African J. Geol. 110:275-294. doi:10.2113/gssajg.110.2-3.275

van Wees JD, Cloething S (1996) 3D Flexure and intraplate compresison in the Norht Sea Basin. Tectonophyiscs 266:343-359.

von Nicolai C, Scheck-Wenderoth M, Warsitzka M, Schødt N, Andersen J (2013) The deep structure of the South Atlantic Kwanza Basin - Insights from 3D structural and gravimetric modelling. Tectonophsics 694: 139-152. doi: 10.1016/j.tecto.2013.06.016

Waples DW, Waples JS (2004) A review and evaluation of specific heat capacities of rocks, minerals, and subsurface fluids. Part1: Minerals and Nonporous Rocks. Natural Resources Research 14 (2):97-122. doi.org/10.1023/B%3ANARR.0000032647.41046.e7

Watts AB (1978) An Analysis of Isostasy in the World's Oceans 1. Hawaiian-Emperor Seamount Chain. J. Geophys. Res. 83(B12):5989-6004

Watts AB (1992) The effective elastic thickness of the lithosphere and the evolution of foreland basins. Basin Research 4:169-178

Figures

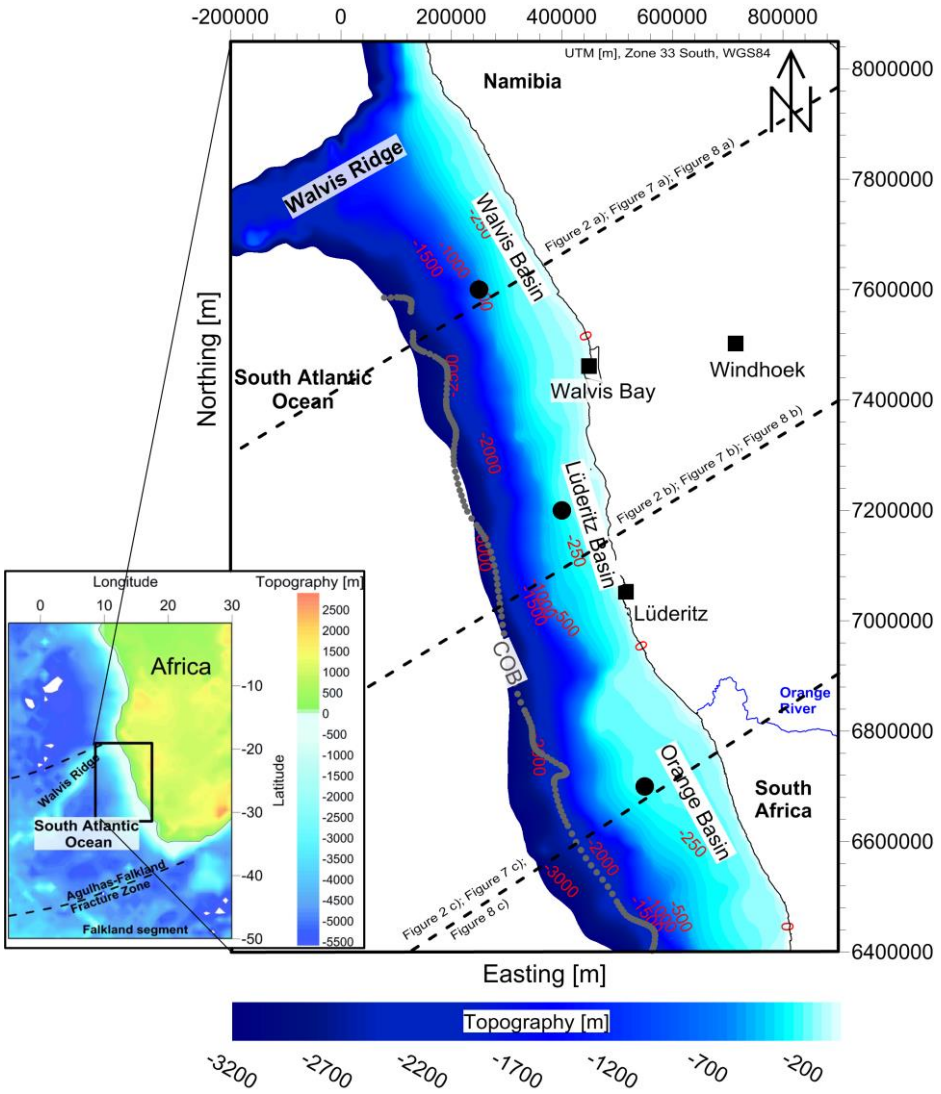

Fig. 1 Map showing the research area, the SW African continental margin (bathymetry after IOC, IHO and BODC, 2003) with continent-ocean boundary (COB, grey dotted line, after Pawlowski, 2008). Black dashed lines mark the profile location used to illustrate the modelling results in Figure 2, Figure 7 and Figure 8. The black solid circles mark the locations of the synthetic boreholes used in Figure 3 and Figure 10 . Coordinate system is UTM in m, WGS 84, zone 33 S. Inset: Overview of the southern African continent and the South Atlantic Ocean

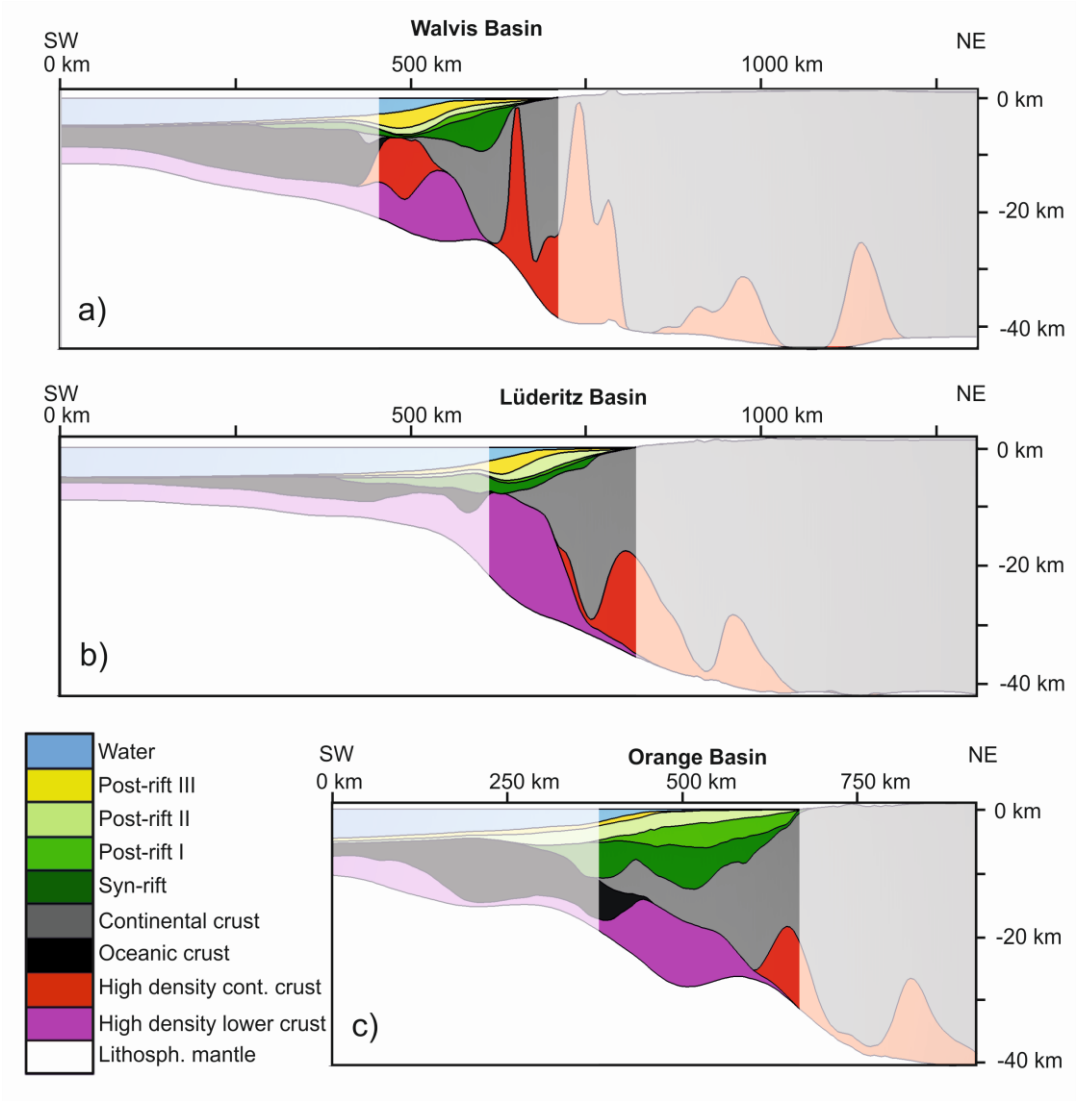

Fig. 2 Profiles across the three major sedimentary basin in the study area: (a) Walvis Basin (b) Lüderitz Basin (c) Orange Basin. The area of the continental margin is highlighted as it is the focus on the study. The cross sections show the distribution of sediments as well as the crustal architecture and the depth to the Moho. See Figure 1 for the exact locations with the study area

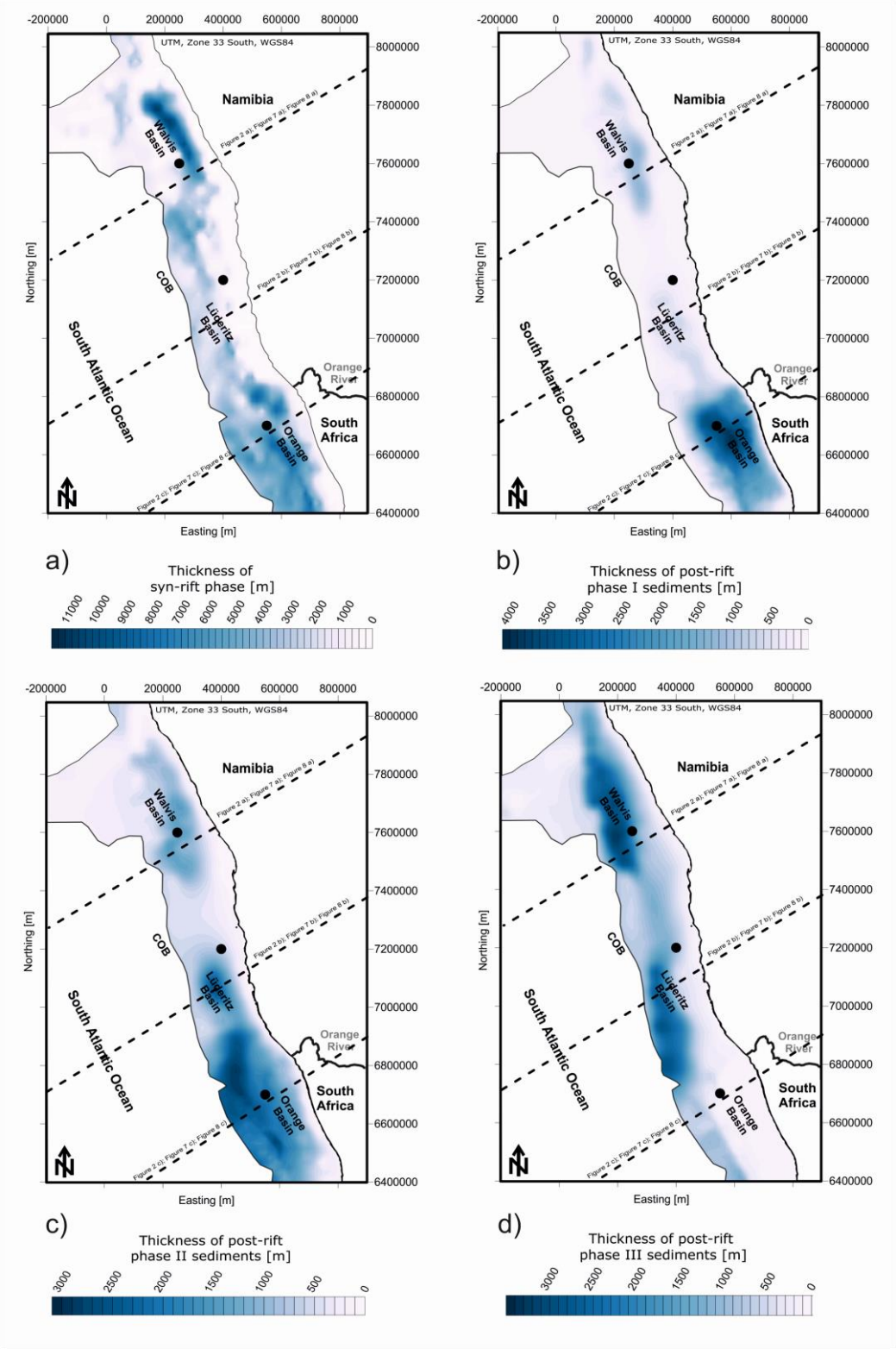

Fig. 3 Isopach maps of the syn-rift unit (a) and of the three post-rift units (b-c). The dashed lines mark the locations of the cross sections shown in Figure 2 as well as Figure 7 and Figure 8. The black dots mark the area of the synsthetic wells further discussed in Figure 4 and Figure 10

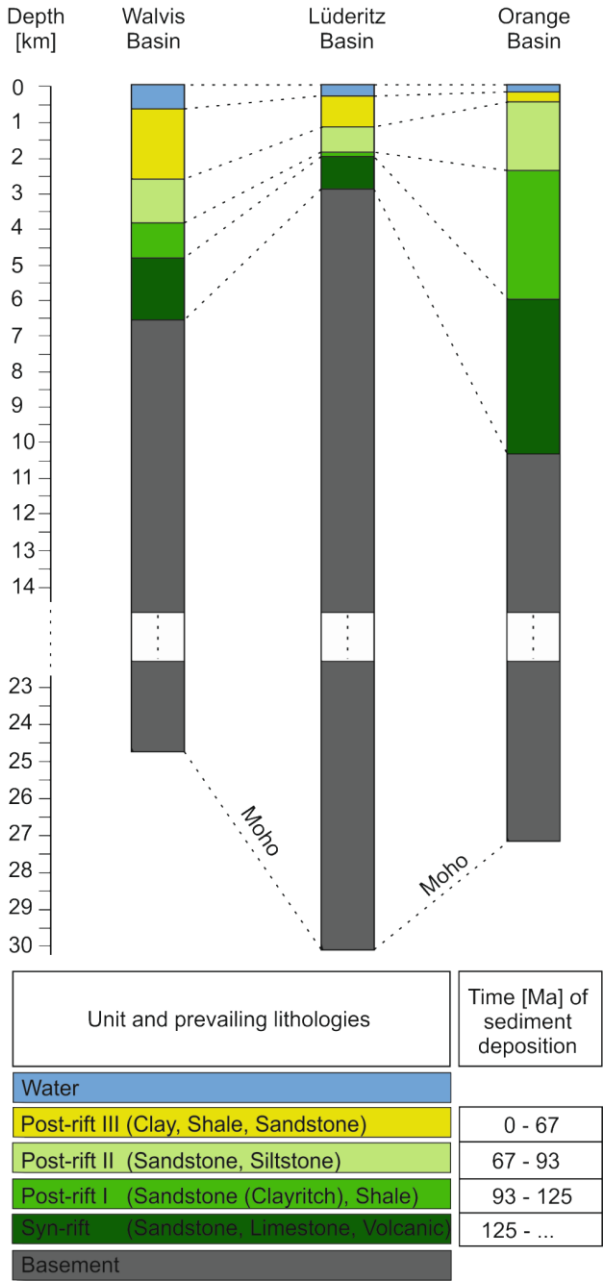

Fig. 4 Stratigraphy of three synthetic wells in each of the major sedimentary basin. See Figure 1 for their locations

Table 1 Names, lithology, ages and assigned physical properties of the individual units used in the 3D forward modelling (after Broad et al. (2006); Hartwig et al. (2012); Hirsch et al. (2007, 2010); Holtar and Forsberg (2000); Maystrenko et al. (2013); Paton et al. (2007); Sclater and Christie (1980), Waples and Waples (2004)

Name	Ages of the units [Ma]	Lithology	Density [kg/m³]	Conduc-tivity [W/mK]	Heat production [µW/m³]	Heat capacity [10^{-3}J/kg K]	Thermal expansion coefficient [*10^{-5}/°C]
Post-rift III	0 - 67	Clay; Shale; Sandstone	2150	1.50	1.00	0.92	
Post-rift II	67 - 93	Sandstone;Siltstone	2420	1.90	1.00	0.88	
Post-rift I	93 - 125	Sandstone (Clay rich); Shale	2550	2.00	1.10	0.84	
Syn-rift		Sandstone; Limestone, Volcanics	2570-2700	2.60	1.30	0.95	
Continental crust			2850	2.80	1.30	0.68	2.80
Lithospheric mantle			3330	3.95	0.03	1.05	3.28
Asthenosphere			3250				

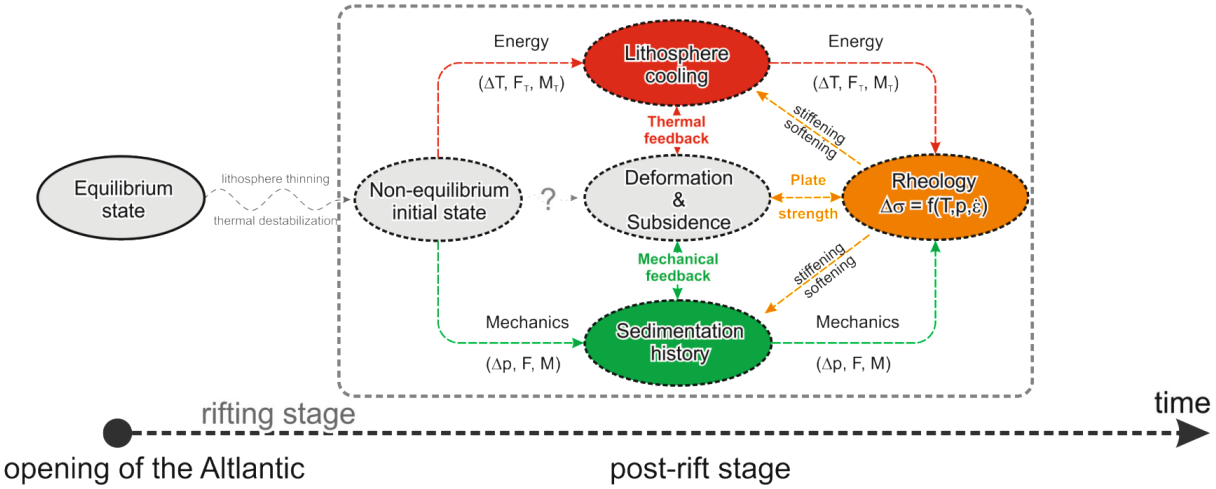

Fig. 5 Scheme of forward modeling approach after Cacace and Scheck-Wenderoth (2014) and Scheck-Wenderoth et al. (2015). An initial perturbation (i.e. lithosphere thinning and thermal destabilization) moves the system out of thermal and mechanical equilibrium. This leads to the generation of internal stresses resulting from variations in the thermal configurations (ΔT) in the forms of a net shear force (F_T) and a bending moment (M_T) as well as to a change in the rheological configuration of the lithosphere. Those variations will trigger vertical crustal

deformation (i.e. subsidence and/or uplift), which will retro-affect the thermal configuration thus promoting new thermal stresses and renewed vertical deformation (i.e. thermal feedback). Sedimentation additionally affects the deformation history through time by imposing a direct load acting on the plate, and by retarding the cooling via thermal blanketing (mechanical feedback). In our approach, we do not consider a rheological model to parameterize the Effective Elastic Thickness (EET), but we constrain its thickness by means of a specified isotherm (T=450°)

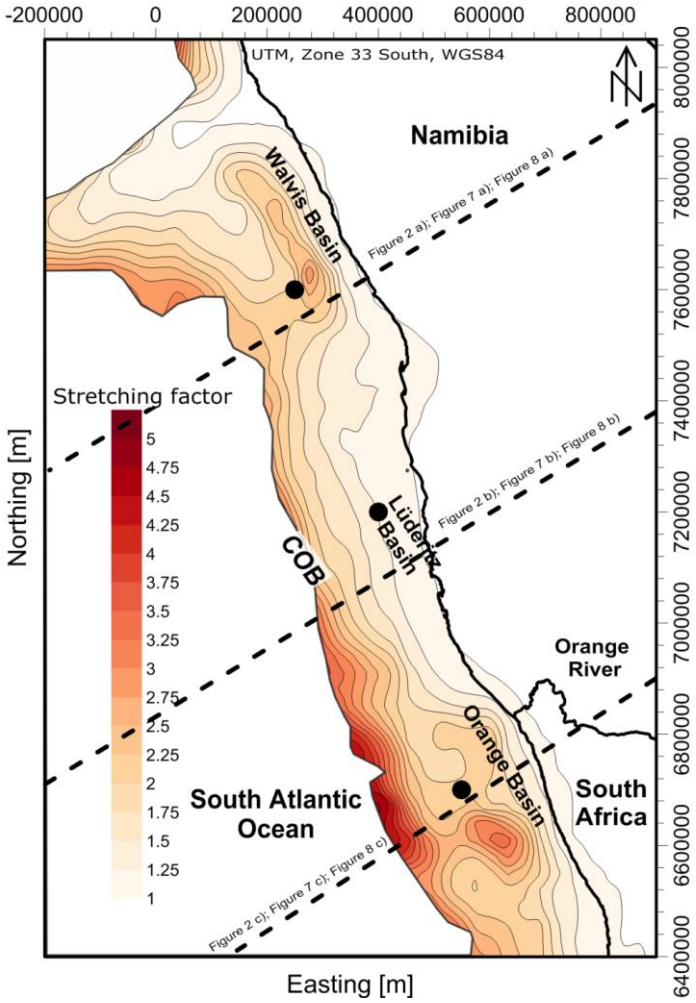

Fig. 6 Map of stretching factor along the continental margin as used to calculate the syn-rift subsidence and the initial conditions at the start of the post-rift phase. In general, there is a decrease in the amount of stretching from west to east with areas of significantly higher stretching factors (up to 3.5) in the areas of the Walvis Basin in the north and the Orange Basin in the south

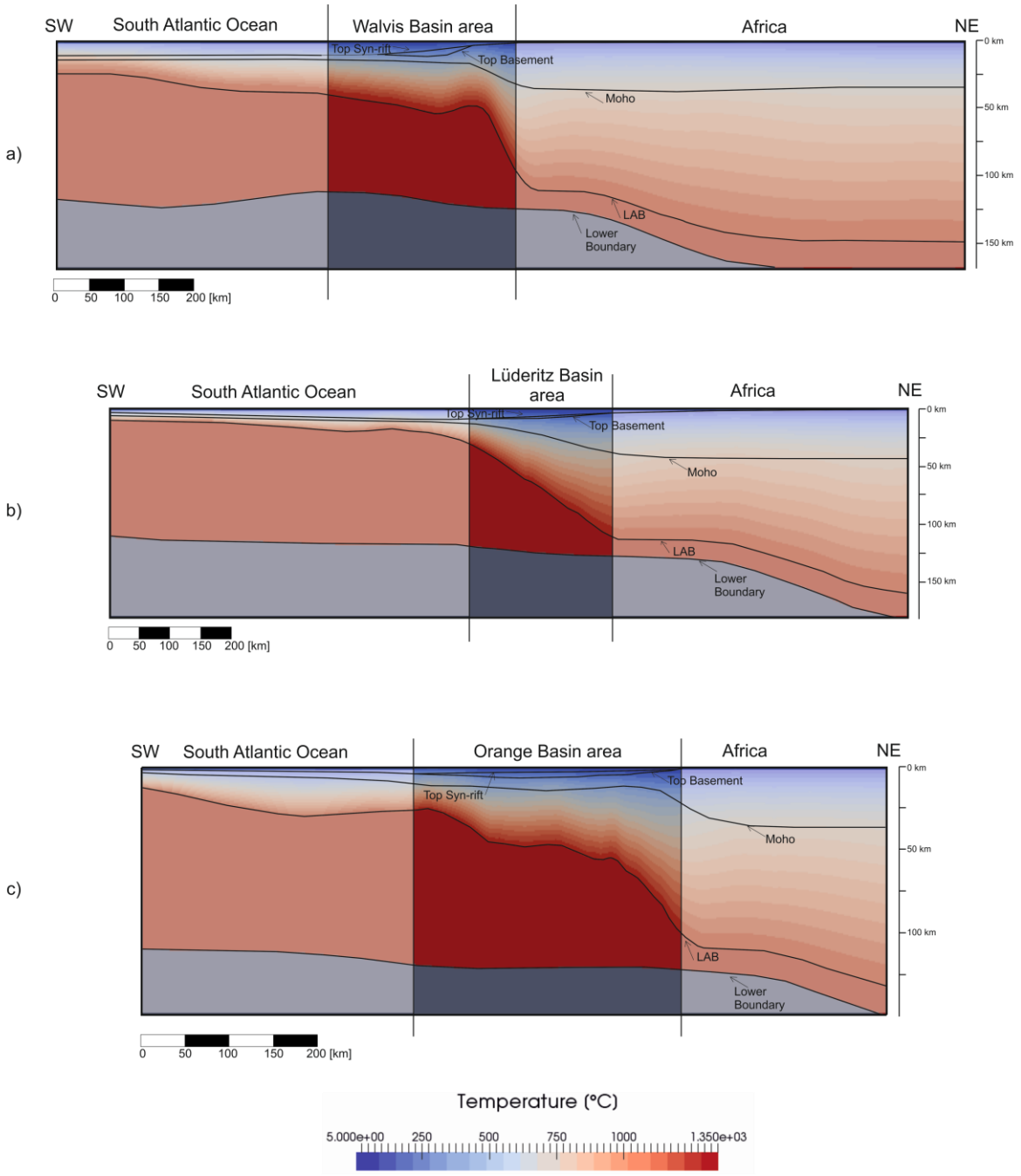

Fig. 7 Temperature profiles across the 3D model at the end of the syn-rift phase (125 Ma). The locations of the profiles are the same as illustrated in Figure 1 and Figure 2. (a) Profile across the Walvis Basin. (b) Profile across the Lüderitz Basin. (c) Profile across the Orange Basin. The margin area is strongly affected by stretching and shallow isotherms that deepen towards the continent

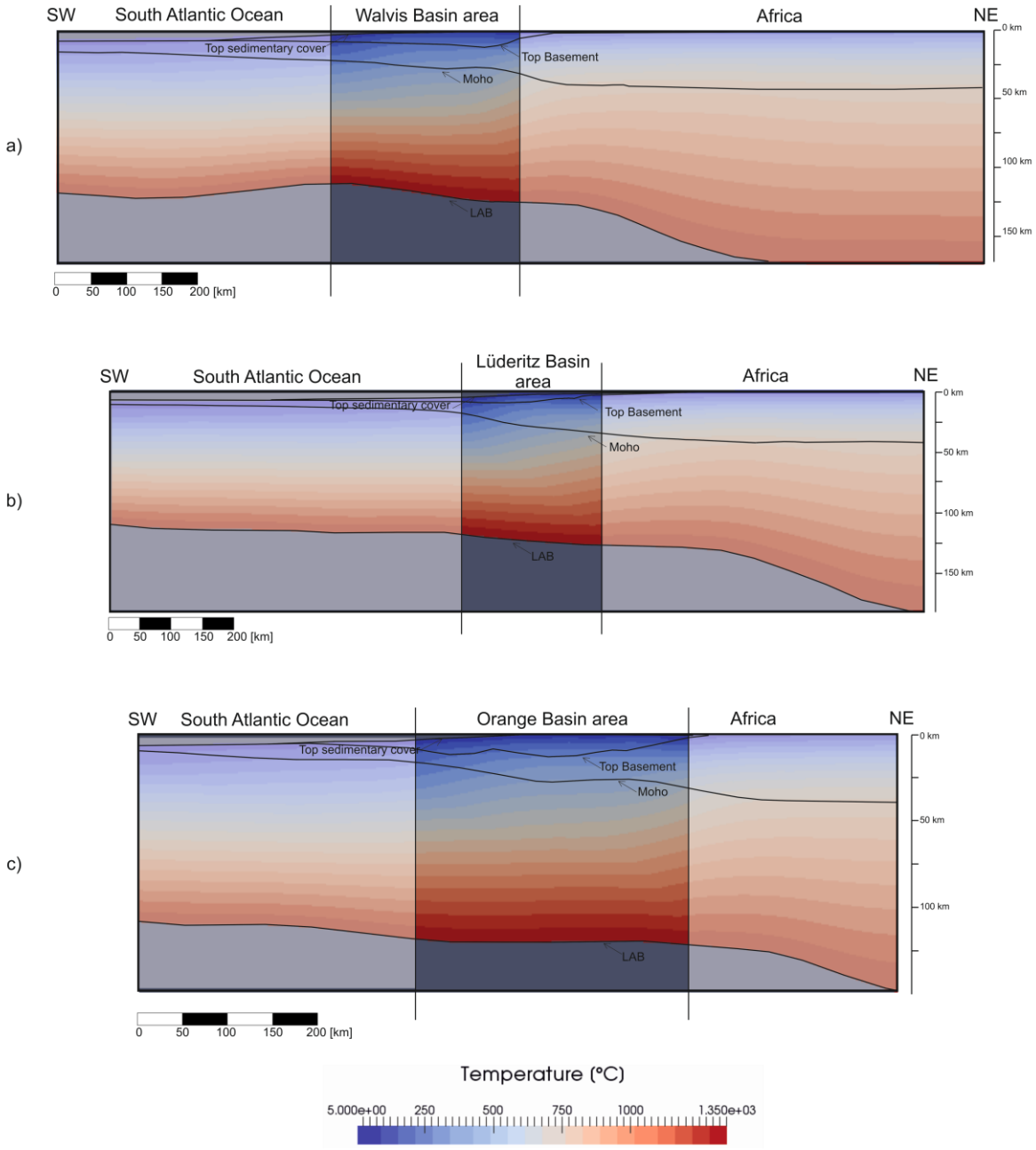

Fig. 8 Temperature profiles, as in Figure 7 but at t = 0 Ma. (see Figure 1 for their locations). (a) Profile across the Walvis Basin. (b) Profile across the Lüderitz Basin. (c) Profile across the Orange Basin. These profiles illustrate the elevated isotherms in the areas of the sedimentary basins

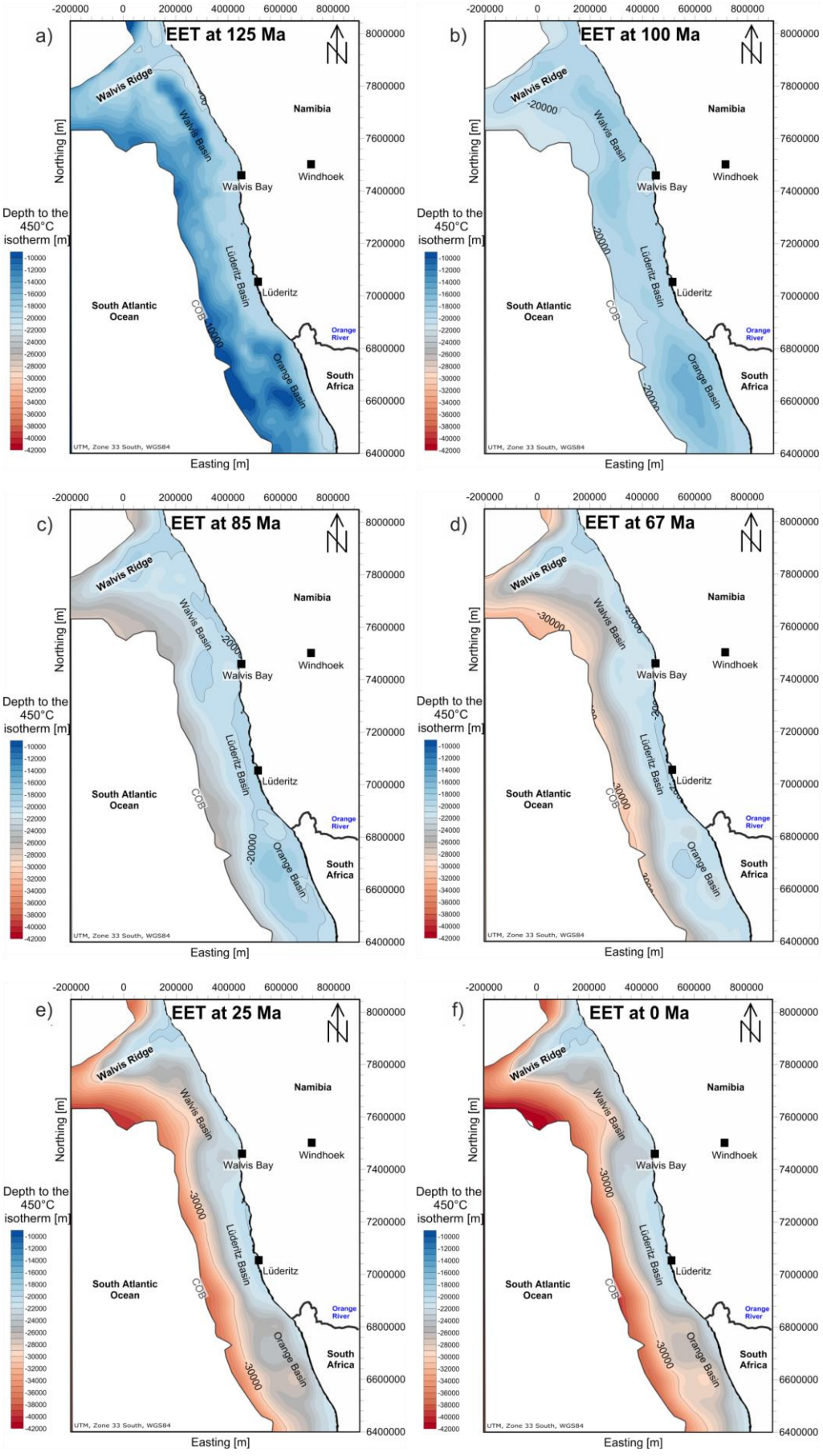
a)
EET at 125 Ma
b)
EET at 100 Ma
c)
EET at 85 Ma
d)
EET at 67 Ma
e)
EET at 25 Ma
f)
EET at 0 Ma
Walvis Ridge
Walvis Basin
Lüderitz Basin
Orange Basin
Namibia
Windhoek
Walvis Bay
Lüderitz
South Atlantic Ocean
South Africa
Orange River
COB
Northing [m]
Easting [m]
Depth to the 450°C isotherm [m]
UTM, Zone 33 South, WGS84

Fig. 9 Evolution of the EET with time. (a) Depth to the EET at 125 Ma. (b) Depth to the EET at 100 Ma. (c) Depth to the EET at 85 Ma. (d) Depth to the EET at 67 Ma. (e) Depth to the EET at 25 Ma. (f) Depth to the EET at 0 Ma. Strong variations in the thickness distribution of the EET are observed during the first 25 Ma after breakup when thermal cooling of the lithosphere has started. Since 100 Ma, the spatial pattern of the EET does not vary significantly, reflecting a rather slower cooling of the lithosphere plate, which approaches equilibrium

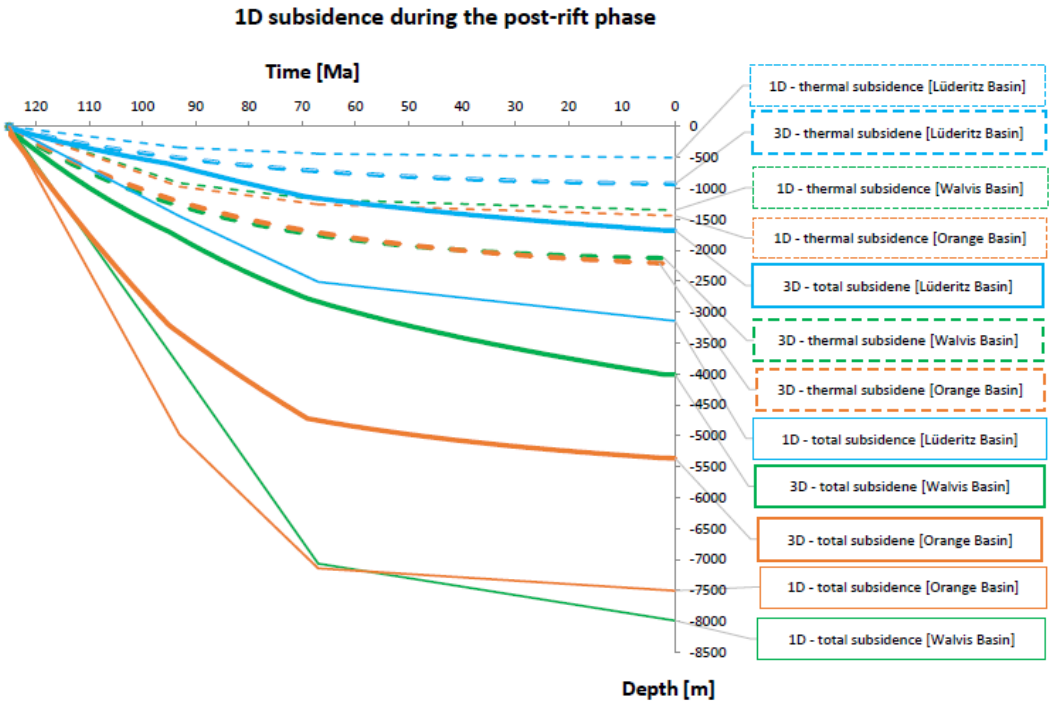

Fig. 10 Comparison between subsidence curves of three synthetic boreholes within the Walvis Basin, Lüderitz Basin and Orange Basin calculated with the 3D forward modelling approach and a spatio-temporal EET and with local isostatic compensation (i.e. EET=0; Dressel et al. 2015). Dashed lines show the thermal subsidence curves with thick lines for the 3D case and thin lines for local isostatic compensation. Solid lines represent the total subsidence curve (i.e. load induced subsidence + thermal subsidence). The space in between the dashed and the solid curves indicate the amount of load induced subsidence. Again, the thick lines show the

subsidence curve for the 3D calculation and the thin lines mark the local isostasy calculation (see Figure 1 for location)

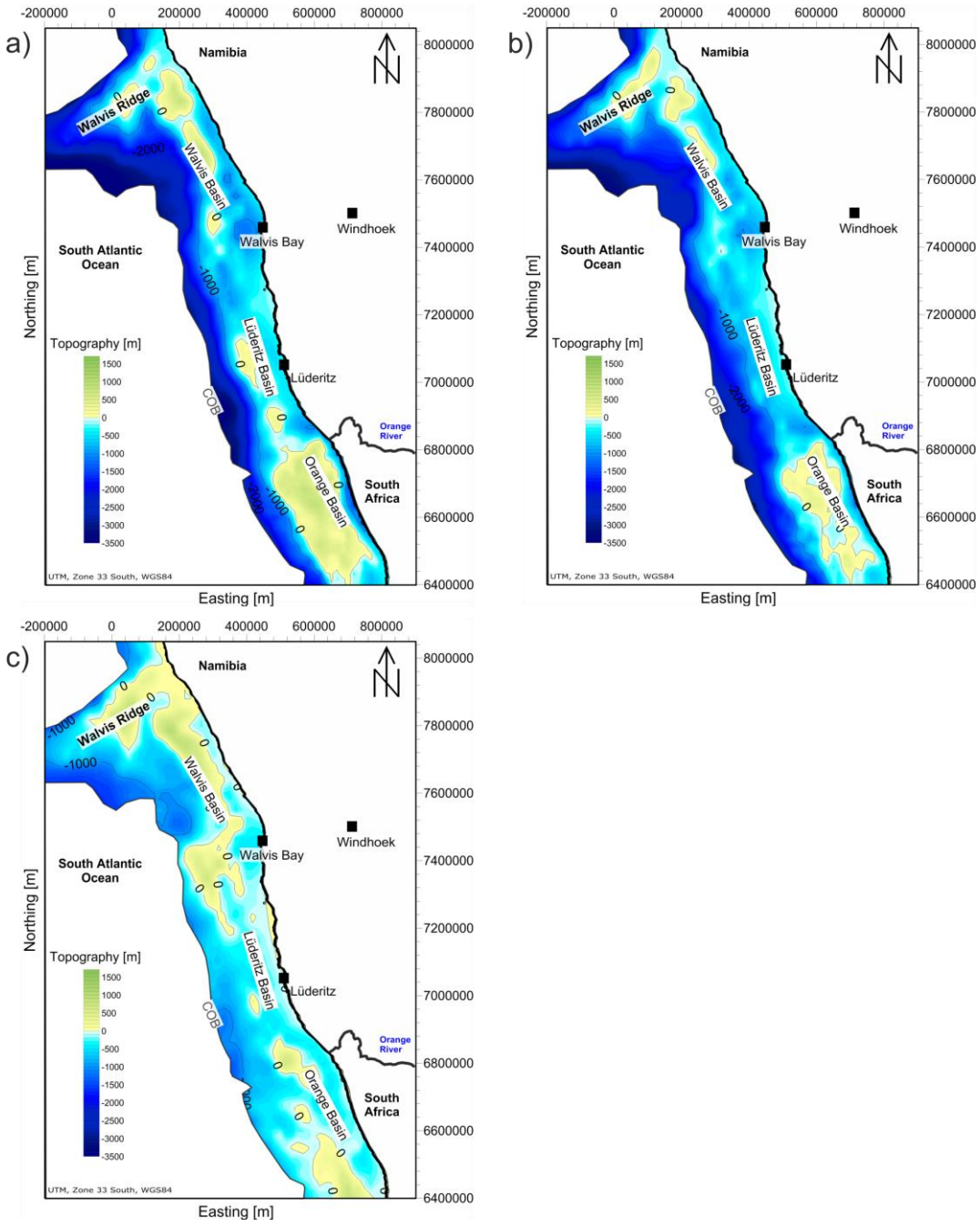

Fig. 11 Modelled paleobathymetries for 67 Ma (a), 93 Ma (b), 125 Ma (c). The maps indicate a positive paleotopography above sea level. The amount of this positive paleotopography varies through time

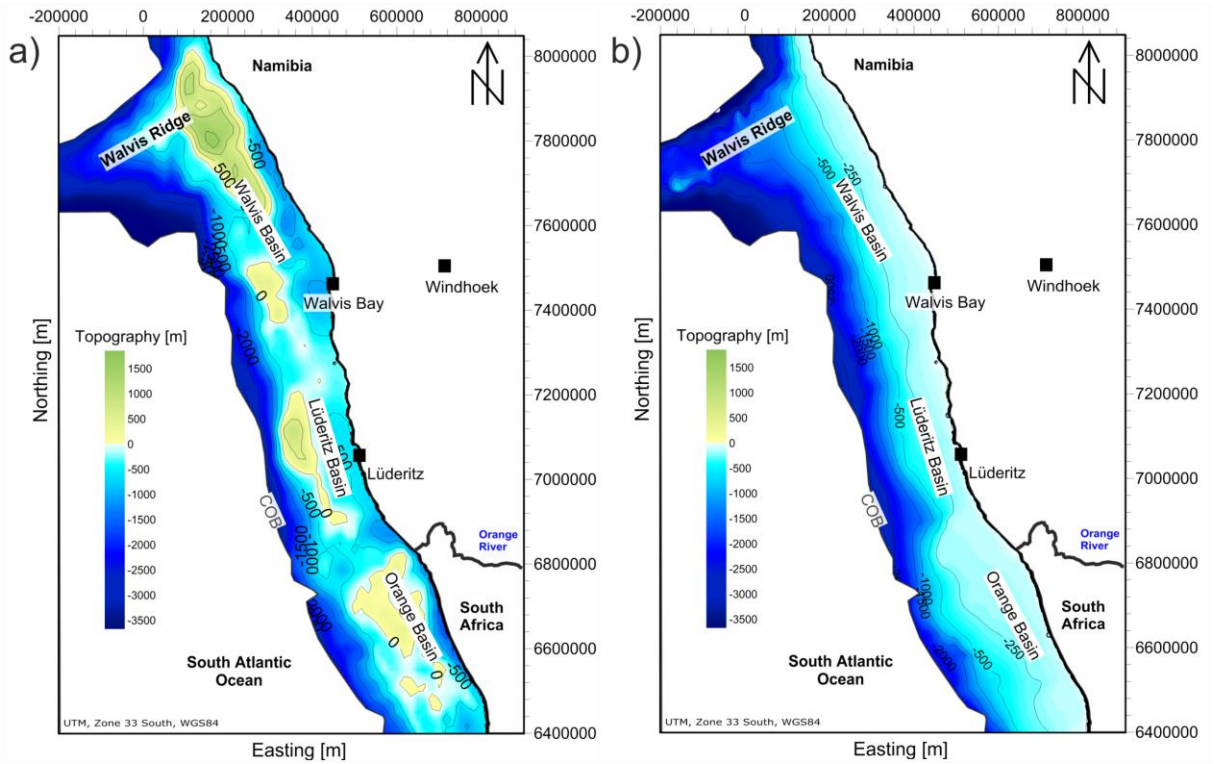

Fig. 12 The maps show the reconstructed bathymetries for present-day (a) and the real present-day bathymetry (after IOC, IHO and BODC, 2003; b). Figure (a) shows elevations above sea-level which are not observed at the real present-day (b)

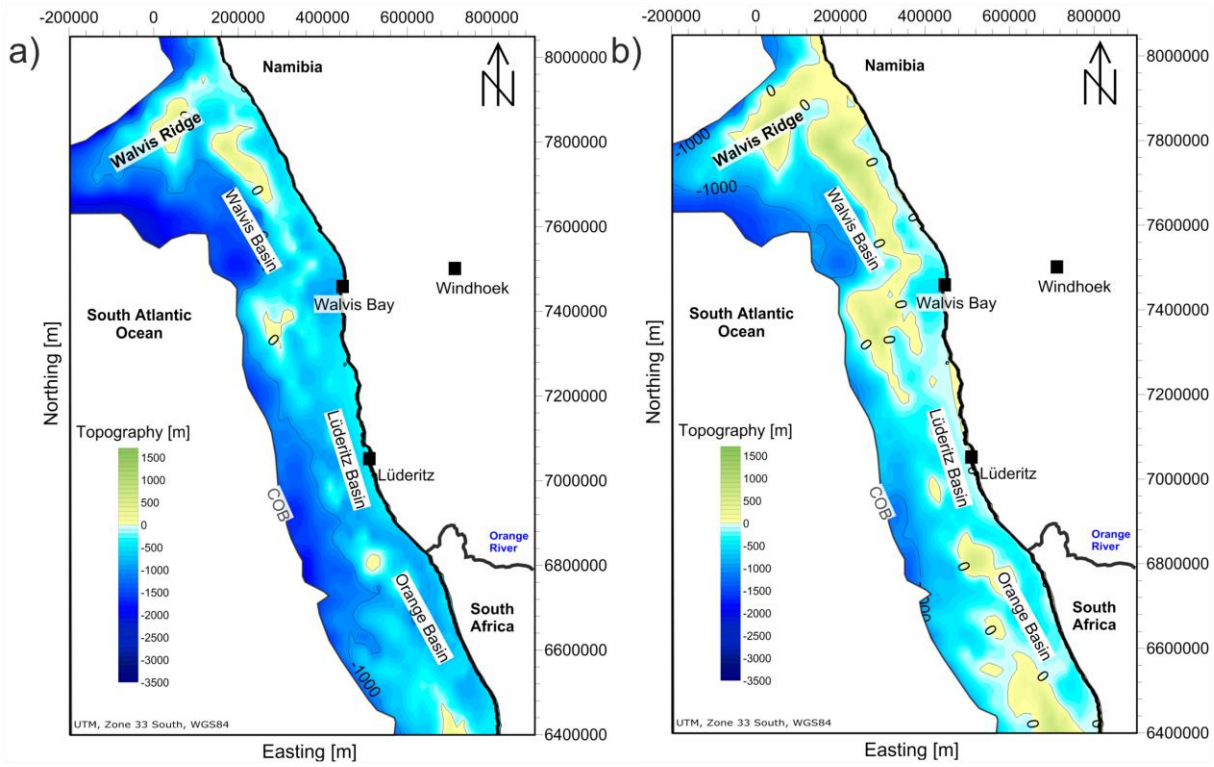

Fig. 13 Comparison between the paleobathymetry at top of the syn-rift unit calculated with an initial configuration of 40 km crustal thickness and 130 km lithospheric thickness (a) with those paleobathymetry calculated with the initial configuration of 35 km for the crustal thickness and 125 m of lithospheric thickness (b)

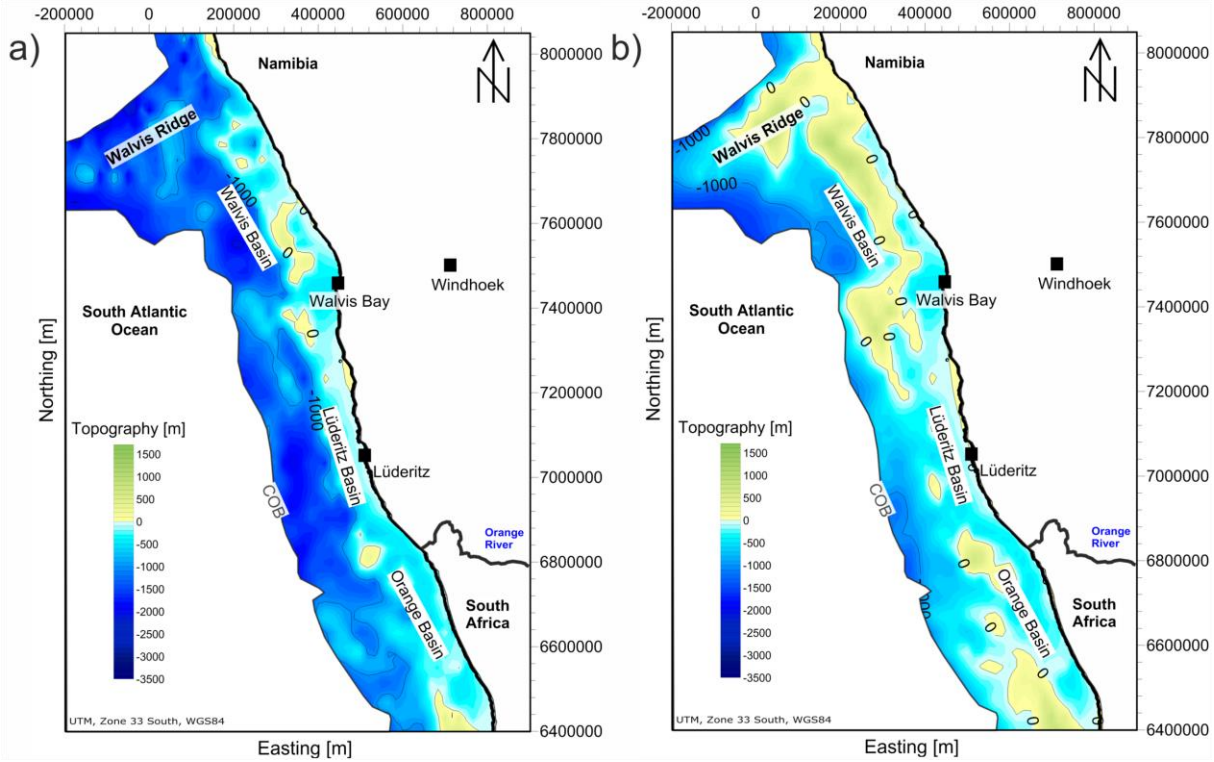

Fig. 14 Comparison between the paleobathymetry at the top of the syn-rift unit calculated assuming lower crustal bodies as part of the mantle (emplacement post-breakup; a) and as part of the crystalline crust (emplacement pre-breakup; b)

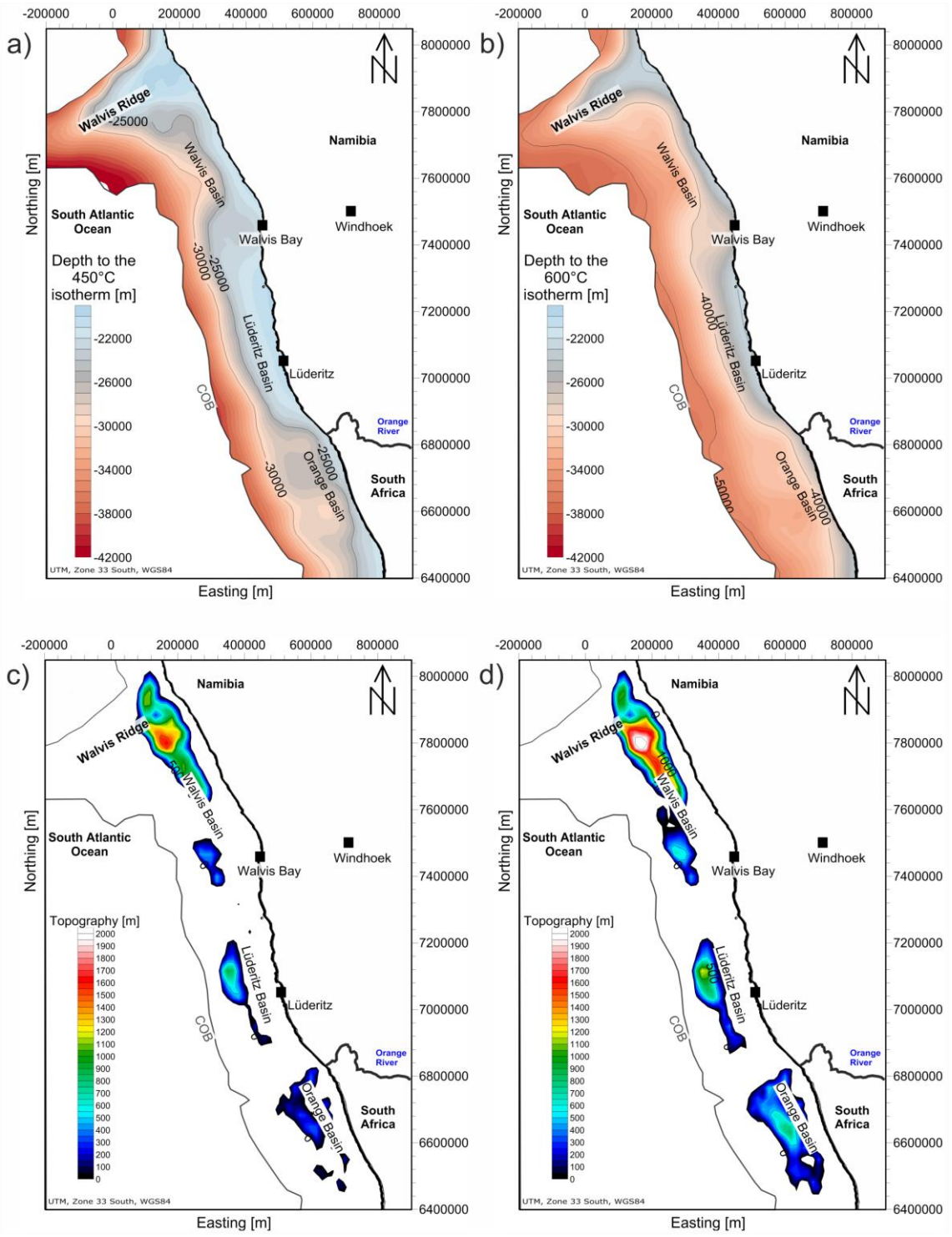

Fig. 15 Map (a) and (b) exemplarily show the depth to EET assuming its base at the 450°C isotherm and 600°C isotherm, respectively. Map (c) shows the paleotopography using an EET=450°C while map (d) illustrates the resulting paleotopography modeled with an EET=600°C. According to the different EETs, the paleotopographies vary in magnitude